DESIGN AND ANALYSIS OF AN OPEN LOOP FIBER-OPTIC GYROSCOPE

A THESIS SUBMITTED TO
THE GRADUATE SCHOOL OF NATURAL AND APPLIED SCIENCES
OF
MIDDLE EAST TECHNICAL UNIVERSITY

BY

MURAT ÖZDEMİR

IN PARTIAL FULFILLMENT OF THE REQUIREMENTS
FOR
THE DEGREE OF MASTER OF SCIENCE
IN
PHYSICS

FEBRUARY 2012

Approval of the thesis:

DESIGN AND ANALYSIS OF AN OPEN LOOP FIBER-OPTIC GYROSCOPE

Submitted by **MURAT ÖZDEMİR** in partial fulfillment of the requirements for the degree of Master of Science in **Department of Physics, Middle East Technical University** by,

Prof. Dr. Canan Özgen _____
Dean, Graduate School of **Natural and Applied Sciences**
Prof. Dr. Mehmet Zeyrek _____
Head of Department, **Physics**
Assoc. Prof. Dr. Hakan Altan _____
Supervisor, **Physics Dept., METU**
Dr. Halil Berberoğlu _____
Co-Supervisor, **Physics Dept., METU**

Examining Committee Members

Assoc. Prof. Dr. Serhat Çakır _____
Physics Dept., METU
Assoc. Prof. Dr. Hakan Altan _____
Physics Dept., METU
Assist. Prof. Dr. Behzat Şahin _____
Electrical and Electronics Engineering Dept., METU
Dr. Halil Berberoğlu _____
Physics Dept., METU
Ali Galip Yıldırım, MSc _____
TÜBİTAK-SAGE

Date: _____

I hereby declare that all information in this document has been obtained and presented in accordance with academic rules and ethical conduct. I also declare that, as required by these rules and conduct, I have fully cited and referenced all material and results that are not original to this work.

Name, Last name: Murat ÖZDEMİR

Signature :

ABSTRACT

DESIGN AND ANALYSIS OF AN OPEN LOOP FIBER-OPTIC GYROSCOPE

Özdemir, Murat
M.Sc., Department of Physics
Supervisor: Assoc. Prof. Dr. Hakan Altan

February 2012, 74 Pages

Sensing rotation has been an essential topic in navigation and many other applications. Gyroscopes based on propagation of light beams over fixed distances have gained interest with the development of the laser. Since the 1970s, with the development of fiber optics these laser based gyroscopes have developed into compact devices, which can fit in the palm of your hand. In this thesis, we describe and analyze the development of a fiber-optic gyroscope. Fiber optic gyroscopes (also called fiber gyro or FOG) have been under development for different types of applications for more than 30 years all around the world. The physical basis of the fiber gyro is the Sagnac effect that was discovered in the early 1900s and is named after its discoverer.

In this work, we first explain the principle of operation of the Sagnac effect and we derive the fundamental formulations in order to have an analytical understanding of the theory. Then, we examine the fiber optic gyro configuration component by component, starting with the laser diode pumped broadband light emitting Erbium-doped superfluorescent source. In addition, the principle of phase modulation, electro-optic phase modulators, fiber optic cables and fiber winding techniques, such as quadrupolar winding is explained within the context of development of the FOG.

The FOG that was assembled was based on circulation and sensing of broadband light centered around 1550nm. The fiber coil was 5km long in order to increase sensitivity in the FOG device. Since single-mode fibers were used steps were taken to ensure successful operation even with polarization dependent errors. The constructed system demonstrated a low sensitivity with a large uncertainty while sensing typical rotation rates. Reasons behind the errors and low sensitivity, as well as improvements that can be made are discussed.

Keywords: Fiber-Optic Gyroscope , FOG, Open Loop, Single Mode Fiber, Electro-Optic Phase Modulator

ÖZ

AÇIK DÖNGÜ FİBEROPTİK DÖNÜÖLÇER TASARIMI VE ANALİZİ

Özdemir, Murat
Yüksek Lisans., Fizik Bölümü
Tez Yöneticisi: Doç. Dr. Hakan Altan

Şubat 2012, 74 Sayfa

Dönü ölçmek seyrüsefer ve birçok benzer alanda her zaman önemli bir konu olmuştur. Işığın sabit mesafeleri katetmesi temeli üzerine kurulan FOD'lar lazerlerin gelişimiyle ilgi görmeye başladılar. Lazer temelli dönü ölçerler, 1970'lerden itibaren, fiber-optikteki gelişmelerle avucunuza sığabilecek kompakt cihazlar şeklinde geliştirilmiştir. Bu tezde bir fiber-optik dönüölçerin gelişimi anlatılmış ve incelenmiştir. Fiber-optik dönüölçerler (FOD) 30 yılı aşkın bir süredir çeşitli uygulamalar için geliştirilmektedir. FOD'un temeli 1900'lerde keşfedilen Sagnac etkisidir ve mucidinin adıyla anılmaktadır.

Bu çalışmada öncelikle, Sagnac etkisinin çalışma prensibi anlatılmış ve temel formülasyonlar çıkarılmıştır. Daha sonra FOD yapısı bileşen bileşen incelenecektir. Lazer diyotla pompalanmış geniş spektrumlu erbium dope edilmiş fiber kullanılarak oluşturulan ışık kaynağı, elektro-optik faz modülatörleri, fiber-optik kablolar ve fiber kablo sarma teknikleri detaylı ve gerekliliklerini açıklayacak şekilde anlatılmıştır.

Kurulan FOD yapısı, 1550nm etrafıdaki geniş spektrumlu ışığın döngüyü dolaşması ve algılanması temeli üzerine kurulmuştur. Fiber boyu, hassasiyetin arttırılması için 5kmdir. Tek modlu fiber kullanıldığından, polarizasyona dayalı

hatalara rağmen başarılı bir FOD sistemi kurmak için, farklı yöntemler kullanılmıştır. Kurulan sistem yüksek bir belirsizlikle düşük hassasiyet göstermekle beraber tipik dönü değerlerini ölçmüştür. Bu düşük hassasiyet ve hatalara sebep olan sebepler incelenmiş ve tartışılmıştır.

Anahtar kelimeler: fiber-optik dönü ölçer, FOD, açık döngü, tek modlu fiber, elektro-optik faz modülatörü

To my dear Family

ACKNOWLEDGMENTS

I am most thankful to my supervisor Assoc. Prof. Dr. Hakan Altan and my co-supervisor Dr. Halil Berberoğlu for sharing their invaluable ideas and experiences on the subject of my thesis.

I am very grateful to TÜBİTAK-SAGE throughout the production of my thesis.

I would like to forward my appreciation to all my friends and colleagues especially Ali Galip YILDIRIM, Hüseyin Caner BECER, Melih ÇETİN and Salih ZENGİN who contributed to my thesis with their continuous encouragement.

TABLE OF CONTENTS

ABSTRACT ..... **IV**

ÖZ ..... **VI**

ACKNOWLEDGMENTS ..... **IX**

TABLE OF CONTENTS ..... **X**

LIST OF TABLES ..... **XIII**

LIST OF FIGURES ..... **XIV**

LIST OF ABBREVIATIONS ..... **XVI**

1 INTRODUCTION **1**

1.1 Historical Review **1**

1.2 Gyroscopes, General Overview and Comparison **2**

1.2.1 Basic Theory of Ring Laser Gyroscopes 3

1.2.2 Basic Theory of Fiber Optic Gyroscopes 4

1.3 Scope of the Thesis **4**

2 BACKGROUND **6**

2.1 Sagnac Effect **6**

2.1.1 Physical Explanation 6

2.1.2 Derivation of the Scale Factor 7

2.2 Bias Modulation **9**

2.2.1 Rotation Sensitivity 9

2.2.2 Square Wave Bias Modulation 10

2.2.3 Appropriate Modulation Frequency 13

2.3 Reciprocity **13**

2.3.1 Principle of Reciprocity 13
2.3.2 Problem of Polarization Non-Reciprocity 15
2.3.3 Use of a Depolarizer 16

3 DESIGN OF A FOG 18

3.1 Components of a FOG 18
3.1.1 Light Source 19
3.1.1.1 Superluminescent Diode 20
3.1.1.2 Erbium Doped Superfluorescent Fiber Sources (SFS) 21
3.1.2 2x2 Coupler 23
3.1.3 Polarizer 25
3.1.4 Electro-Optic Phase Modulator 26
3.1.5 Multifunctional Integrated Optic Chip (MIOC) 31
3.1.6 Fiber Coil 35
3.1.7 Detector 38

4 ASSEMBLING AND TEST OF A FIBER-OPTIC GYROSCOPE 40

4.1 Assembling and Verification 41
4.1.1 Fiber Splicing 41
4.1.2 Optical Spectrum Analyzer (OSA) Measurements of the Erbium Doped Superfluorescent Fiber Source 46
4.1.3 Optical Loss Analysis 48
4.1.4 Polarization Extinction Ratio (PER) Analysis 50
4.1.5 Optical Time Domain Reflectometry (OTDR) Measurements 53
4.2 The Measurement Setup 56
4.2.1 Peripheral Devices 56
4.2.2 Transimpedance Amplifier (TIA) 58
4.3 Testing the FOG 59
4.3.1 Calculation of the Appropriate Modulation Frequency 59
4.3.2 Characterization of the Phase Modulator 60
4.3.3 Measurements with the Rate Table 62
4.3.4 Experimental Evaluation of the Scale Factor 66

5 DISCUSSION AND CONCLUSION 68

5.1 Conclusions 68
5.2 Future Work 69

6 REFERENCES 71

LIST OF TABLES

Table 3-1 Light source requirements for FOG 20
Table 3-2 Light source design parameters 22
Table 3-3 V_{π} values for different phase modulator configurations 31
Table 4-1 List of components used 41
Table 4-2 PER Measurements 52
Table 4-3 Peripheral Devices 57
Table 4-4 Values for components of TIA 59
Table 4-5 Input rate vs. output of the FOG 66
Table 4-6 Scale factor for each rotation rate 66

LIST OF FIGURES

Figure 1-1 Special type of ring laser gyroscope 3
Figure 1-2 Typical Fiber Optic Gyroscope 4
Figure 2-1 Path Length Difference Generated by the Sagnac Effect 7
Figure 2-2 Illustration of Sagnac Effect 7
Figure 2-3 Interferogram at detector 11
Figure 2-4 Square wave bias modulation[17] 12
Figure 2-5 Reciprocal FOG configuration [17] 14
Figure 2-6 Reciprocal FOG configuration with polarizer 15
Figure 2-7 Lyot depolarizer (wave plate) 16
Figure 2-8 Lyot depolarizer (PMF) 16
Figure 3-1 Minimum Reciprocal FOG configuration 18
Figure 3-2 Erbium doped superfluorescent fiber source (SFS) configuration 22
Figure 3-3 Fiber Optic 2x2 Coupler 23
Figure 3-4 FOG Configuration 24
Figure 3-5 Side polishing technique [31] 24
Figure 3-6 Fiber-optic polarizer and linear polarization 25
Figure 3-7 Schematic of the fiber polarizer 26
Figure 3-8 Basic phase modulator design on $LiNbO_3$ crystal 27
Figure 3-9 Fabricating waveguides on $LiNbO_3$ by titanium indiffusion 28
Figure 3-10 Light beams with different polarization states entering an x-cut y-propagating phase modulator 30
Figure 3-11 Single polarization propagation through a proton exchange waveguide 32
Figure 3-12 The multifunctional integrated optic chip (MIOC) 33
Figure 3-13 FOG configurations (a) with conventional phase modulator (b) with MIOC 34
Figure 3-14 Push-pull phase modulation 34
Figure 3-15 200m PMF fibers on 25mm and 30mm inner diameter coils 35

Figure 3-16 Propagation of linearly polarized light through (a) single mode fiber (b) single mode polarization maintaining fiber [17] 36
Figure 3-17 Cross section of (a) helical (b) quadrupolar wound fiber coils 37
Figure 3-18 Three different brand InGaAs PIN Photodiodes (fiber pigtailed) 39
Figure 4-1 Single mode fiber structure 42
Figure 4-2 Tools necessary to prepare fibers for splicing 43
Figure 4-3 Cleaving of a stripped fiber (a) before and (b) after 44
Figure 4-4 (a) Fujikura FSM-50S fusion splicer (b) prepared fibers ready for splicing 44
Figure 4-5 (a) alignment of fibers by image processing (b) fusion splice by arc created at tips of electrodes (c) loss estimation and proof test 45
Figure 4-6 FOG components spliced together 46
Figure 4-7 Yokogawa AQ6373 optical spectrum analyzer 47
Figure 4-8 OSA measurements at the output of (a) 980nm laser diode (b) 1550nm Er-doped SFS 47
Figure 4-9 Optical spectra for various pump currents 48
Figure 4-10 Thorlabs ITC4001 laser diode / temperature controller 48
Figure 4-11 Laser diode I-P characterization 49
Figure 4-12 Optical power measurement setup 49
Figure 4-13 Optical power analysis of the FOG 50
Figure 4-14 PER measurement setup 51
Figure 4-15 PER measurement procedure 52
Figure 4-16 PER analysis of the FOG 53
Figure 4-17 Yokogawa AQ7270 OTDR 54
Figure 4-18 OTDR measurement of the fiber coil 54
Figure 4-19 Test Setup 56
Figure 4-20 Test setup diagram 57
Figure 4-21 TIA Circuit 58
Figure 4-22 Interferogram at the detector 61
Figure 4-23 Phase modulator V_{π} characterization curve 61
Figure 4-24 FOG on the rate table 62
Figure 4-25 Output of detector at various rate inputs 64
Figure 4-26 Input rate vs. output of the FOG 65

LIST OF ABBREVIATIONS

FOG:	Fiber optic gyroscope
MTBF:	Mean time between failure
RLG:	Ring laser gyroscope
PNR:	Polarization non-reciprocity
PMF:	Polarization maintaining fiber
MIOC:	Multifunctional integrated optic chip
SNR:	Signal to noise ratio
UV:	Ultra violet
Er:	Erbium
SLD:	Superluminescent diode
ppm:	Part per million
SFS:	Superfluorescent fiber source
ASE:	Amplified spontaneous emission
PER:	Polarization extinction ratio
$LiNbO_3$:	Lithium Niobate
Ti:	Titanium
TE:	Transverse electric
TM:	Transverse magnetic
Si:	Silicon
InGaAs:	Indium gallium arsenide
OSA:	Optical spectrum analyzer
OTDR:	Optical time domain reflectometry
PCBS:	Polarization cube beam splitter
SM:	Single mode

CHAPTER 1

INTRODUCTION

Fiber optic gyroscopes (FOG) have been under development for different applications for the last thirty years. FOGs rely on the Sagnac effect which was named after its discoverer in the early 1900s. The Sagnac effect states that there will be a phase shift between counter propagating optical waves due to rotation of the medium [1]. This discovery laid the foundation to today's wide range FOGs available from tactical grade to inertial/space grade.

There are tremendous numbers of applications for FOGs. Navigation, surveying, oil well drilling, space craft stabilization, car stabilization and any type of platform stabilization can be given as examples to the areas where FOGs are widely used.

1.1 Historical Review

In 1913, Sagnac [1] used a ring interferometer and showed that a phase difference between two counter propagating paths is induced by rotation. The outcome of this demonstration was not even close to the sensitivity of the practical FOGs which are used nowadays. In 1925, Michelson and Gale [2] decided to increase the sensitivity of the ring interferometer by increasing its perimeter to almost 2km. Although they managed to sense the earth rotation, again it was not a practical device since it could not deliver enough sensitivity out of compact sizes. Getting a good sensitivity out of a compact device has become a challenging issue in those years. Scientists were pursuing a way to replace the spinning wheel mechanical gyroscope which had moving parts. These gyroscopes were used for many different purposes such as navigation and stabilization purposes. Even though, they are still used today, optical gyroscopes are preferred as replacements. In 1962 Rosenthal was the first to come up with the idea of recirculating counter propagating waves many times in a resonant path

instead of just once as it was in the Sagnac interferometer. He proposed to use a ring laser cavity to increase the sensitivity [3]. This idea was first implemented by Macek and Davis [4] in 1963 and this was practically the first demonstration of the ring laser gyroscope (RLG). Since then RLGs have been developed and are in use in many inertial applications such as navigation, stabilization, surveying, etc[5][6].

In the 1970s a huge effort had been devoted to the development of the telecommunication industry. These efforts covered the development of low-loss fiber optic cables, stable solid-state semiconductor light sources, fiber optic components and detectors which were the main necessities for this industry. With all these developments it had become possible to use multi-turn fiber optic coils instead of ring lasers to increase the sensitivity of the gyroscopic device. Vali and Shorthill [7] were the first to demonstrate the fiber optical gyroscope in 1976. Since then, a lot of research have been done in order to reduce the size of the FOGs and improve their sensitivity [8].

1.2 Gyroscopes, General Overview and Comparison

Before the invention of sensing rotation with light, rate sensing requirements were fulfilled with mechanical gyroscopes which rely on the angular momentum created with a spinning wheel. However, these conventional gyroscopes were quite sensitive to environmental effects and they had, moving parts, which caused low mean time between failure (MTBF) and the necessity of maintenance.

In the past years development of optical gyroscopes has attracted a lot of interest because of their solid state structure, reliable performance, low cost and immunity to mechanical effects which is not so with the conventional spinning mass gyroscopes. Both ring laser gyroscopes and fiber optic gyroscopes rely on the basis that counter propagating optical waves create a difference in propagation time in a closed optical path. Light waves propagating in opposite directions acquire a phase difference that is induced by variance in path length caused by rotation. As mentioned before, this difference is called the Sagnac effect which forms the basis of all optical gyroscopes [9].

Measurement of the Sagnac effect in RLGs and FOGs are made with quite different techniques. These differences serve as the distinction of the two kind of optical gyros and determines their power requirements, size, weight, cost and performance [10].

1.2.1 Basic Theory of Ring Laser Gyroscopes

RLGs come in various designs [11]. Typically, a laser beam propagates in free-space (air) over a recirculating path. Another example of an RLG is one where the recirculating cavity is actually the gain medium of the laser.

This type of RLG, as in Figure 1-1 consists of a triangular or square cavity made from some glass ceramic compound filled with a helium/neon mixture because of its short coherence length and index of refraction close to 1.0. Electrodes provide gain for this lasing medium and counter propagating waves are generated around the cavity. There must be an integral number of wavelengths around the path so that the optical path supports lasing and oscillation occurs at that frequency. The size of the cavity is adjusted so that it supports oscillation optimal to the lasing media [12][11] .

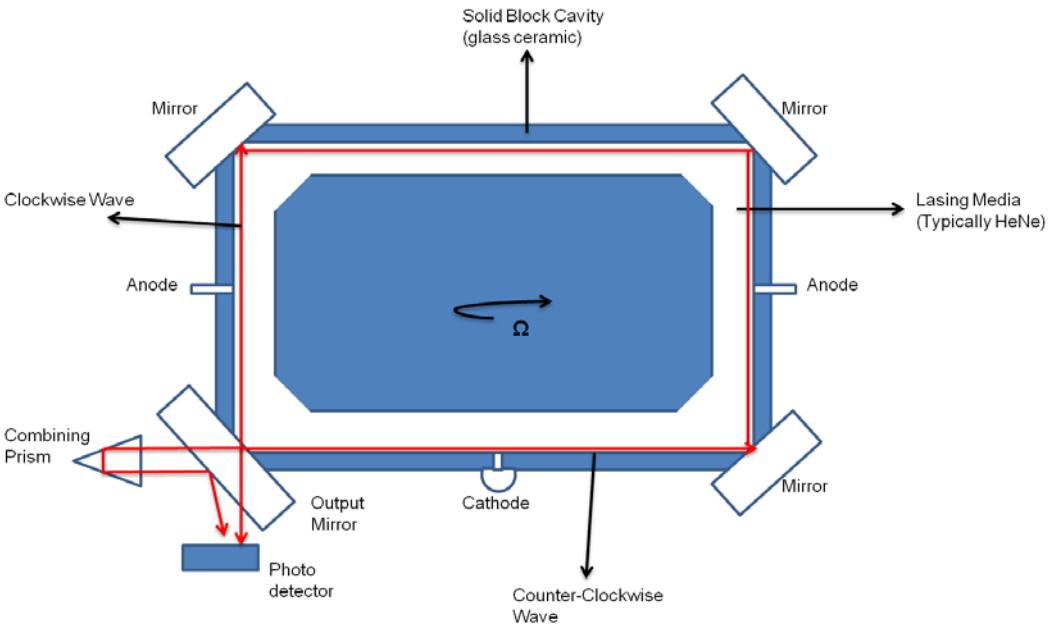

Figure 1-1 Special type of ring laser gyroscope

The output of the RLG is formed by using a combining prism, which creates two collinear beams to form a fringe pattern detected by the photo detector. At the detector signal, number of beats per some time interval is proportional to the rotation rate and the fringe movement determines the direction of rotation [13].

1.2.2 Basic Theory of Fiber Optic Gyroscopes

In a FOG, the source used is important. Using a laser source has its drawbacks since using a coherent source in the FOG system as shown in Figure 2 can cause unwanted interference effects due to the large propagation distance of the counter propagating beams [14]. Here we give a brief description of the FOG device that we will explain in detail later in Chapter 2. As shown in Figure 1-2, the FOG consists of a light source, which emits low coherence broadband light, two fiber couplers, a polarizer, a piezoelectric or electro-optic phase modulator, the sensing coil and a photo detector. Light split into two branches counter propagate within the sensing coil and acquire a phase difference with the rotation of the coil. When they combine, they interfere with each other forming an interference pattern. Phase difference detected at the detector is directly proportional to rotation rate.

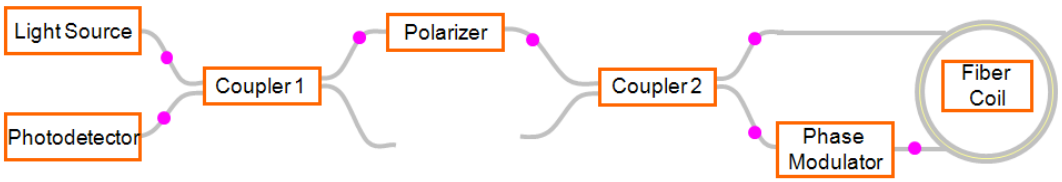

Figure 1-2 Typical Fiber Optic Gyroscope

1.3 Scope of the Thesis

In this thesis, theoretical aspects of the FOG are studied. After explaining fundamentals such as the Sagnac effect, bias modulation and the concept of reciprocity in FOG, we will discuss the necessary components that are used to assemble one. Alternative approaches to the components will be explained along with their advantages and disadvantages.

Later, after having discussed the necessary tools and methods for splicing fiber-optic components we will explain key points to assembling a FOG. Also validation tests such as spectrum analyzer measurements, optical power analysis, polarization extinction ratio measurements and optical time domain reflectometry measurements will be explained with detailed test results.

Test setup in our laboratory is described with pictures and diagrams. Finally, data collected from the rotating FOG is analyzed in order to obtain a scale factor.

CHAPTER 2

BACKGROUND

In this chapter, the theory behind the fiber optic gyroscopes is explained. In section 2.1, a physical explanation of the Sagnac effect is given and later on, the formulization of the scale factor is derived.

In section 2.2 sensitivity of a fiber optic gyroscope system to rotation is examined and further explanations is given with respect to the requirement of bias modulation and the square wave bias modulation technique.

Finally, reciprocity, which is another very important aspect that enables the correct measurement of the Sagnac effect, is discussed in detail in light of the scope of this thesis.

2.1 Sagnac Effect

2.1.1 Physical Explanation

Fundamentally, “Sagnac Effect” is the answer to the question “What is the operating principle of the fiber optic gyroscope?”. The Sagnac effect, which was named after its discoverer Georges Sagnac, states that there will be a phase difference $\Delta\phi$ proportional to the rotation rate Ω in a ring interferometer [15].

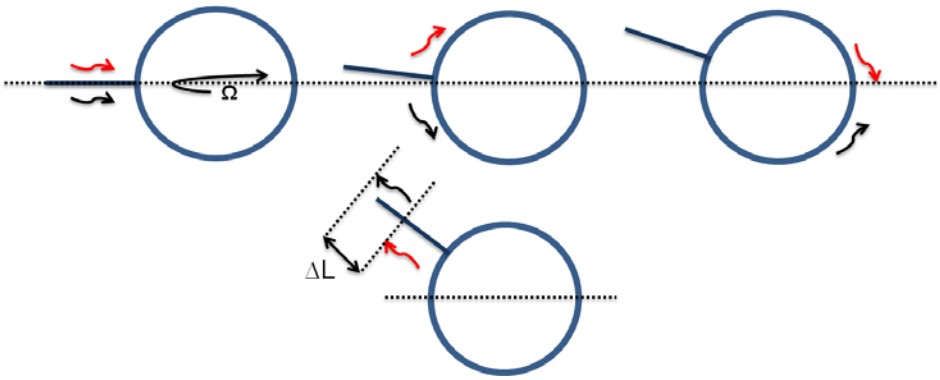

Figure 2-1 Path Length Difference Generated by the Sagnac Effect

In order to get a better understanding one can examine Figure 2-1. Light beams counter propagating in a rotating loop acquire a phase difference because of the difference in paths they travel. This path difference and proportional phase shift is clearly proportional to the loop rotation rate Ω [16].

2.1.2 Derivation of the Scale Factor

Starting with the fact that, in the presence of rotation Ω, two beams travel different fiber lengths and take different times to traverse the total length of the fiber, we can write the effective path lengths as; $L_{cw} = 2\pi R + R\Omega t_{cw}$ and $L_{ccw} = 2\pi R - R\Omega t_{ccw}$ for clockwise length and counter clockwise lengths which light beams travel respectively.

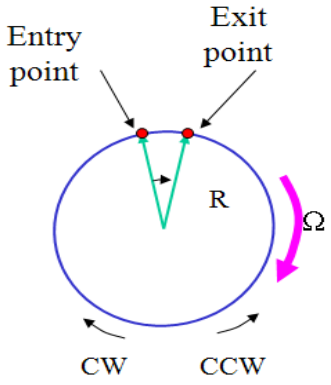

Figure 2-2 Illustration of Sagnac Effect

Therefore, times for light beams to complete one loop would be:

$$t_{cw} = \frac{R(2\pi + \Omega t_{cw})}{c} \tag{2.1}$$

$$t_{ccw} = \frac{R(2\pi - \Omega t_{ccw})}{c} \tag{2.2}$$

Where c is the speed of light in vacuum. Solving separately for t_{cw} and t_{ccw} to the first order in $R\Omega / c$, the wave transit times differ by:

$$\Delta t = t_{cw} - t_{ccw} = 4\pi \frac{R}{c} \cdot \left(\frac{R\Omega}{c} \right) \tag{2.3}$$

Taking into account that fiber coils are wrapped in a coil with N turns:

$$t_{cw} = \frac{R\left(2\pi N + \Omega t_{cw}\right)}{c} \tag{2.4}$$

and

$$t_{ccw} = \frac{R\left(2\pi N - \Omega t_{ccw}\right)}{c} \tag{2.5}$$

Therefore, for a coil with N turns, we find

$$\Delta t = t_{cw} - t_{ccw} = 4\pi \frac{RN}{c} \cdot \left(\frac{R\Omega}{c} \right) \tag{2.6}$$

Substituting coil length $L = 2\pi RN$ and coil diameter $D = 2R$:

$$\Delta t = \frac{LD\Omega}{c^2} \tag{2.7}$$

If we denote the phase shift as $\Delta\phi = \omega\Delta t$, substituting (2.7) into $\Delta\phi$:

$$\Delta\phi = \frac{\omega LD\Omega}{c^2} \tag{2.8}$$

Where, ω is the angular frequency of light,

$$\omega / c = 2\pi / \lambda \tag{2.9}$$

Substituting (2.9) into (2.8) we get:

$$\boxed{\Delta\phi_{Sagnac} = \frac{2\pi LD}{\lambda c}\Omega} \tag{2.10}$$

This result is the phase shift due to the Sagnac effect for light of wavelength λ propagating through a coil of length L and diameter D.
Since in (2.10) Ω stands for the loop rotation rate that is externally applied to the system, the terms on the left give the scale factor for this system [17].

$$\boxed{SF = \frac{2\pi LD}{\lambda c}} \tag{2.11}$$

2.2 Bias Modulation

2.2.1 Rotation Sensitivity

In order to understand these results here an example is shown as to what was derived in the previous section. Our assumptions for the important parameters governing the gyroscope are the following specifications;

- Coil Length, L : 1000m
- Coil Diameter, D : 10cm

- Wavelength, λ :1550nm

Another assumption is that the sensitive axis is exposed to the earth rotation which is 15^o/hour = 7.2×10^{-5}rad/sec

Using equations (2.10) and (2.11);

$$SF = 1.4\ s$$

$$\Delta\phi_{Sagnac} = SF \cdot \Omega = 9.8 \times 10^{-5}\, radian \tag{2.12}$$

Now consider that a detector is placed at the end of the loop, in this case two waves will interfere at this detector with a phase difference of

$$\Delta\phi_{Sagnac} = 9.8 \times 10^{-5}\ \text{radian}$$

The average power of interfering waves is given as:

$$\langle P \rangle = \frac{I_0}{2}(1 + \cos\Delta\phi) \tag{2.13}$$

where I_0 is the detector power when $\Delta\phi = 0$. Then the interference signal will be [17]:

$$\begin{aligned} \langle P \rangle &= \frac{I_0}{2}\left[1 + \cos\left(9.8 \times 10^{-5}\ \text{rad}\right)\right] \\ &\approx \frac{I_0}{2}\left[1 - 5 \times 10^{-9}\right] \end{aligned}$$

As can be seen from the above result we need an extremely sensitive detector to detect this minute change in the power of the beam.

To summarize; the change in detector power, for a gyroscope with above given parameters which is subject to earth rotation, is extremely small. To sense this change, only 5 parts in 10^9 is to be detected which is a very hard task [17].

2.2.2 Square Wave Bias Modulation

The Sagnac phase shift can be well measured by using a modulation on the light source. In order to physically realize the phase shift and understand rotation

sensitivity equation (2.13) is graphed, showing the interferogram in the figure below. In order to have a better understanding about the rotation sensitivity let us examine the interferogram in Figure 2-3.

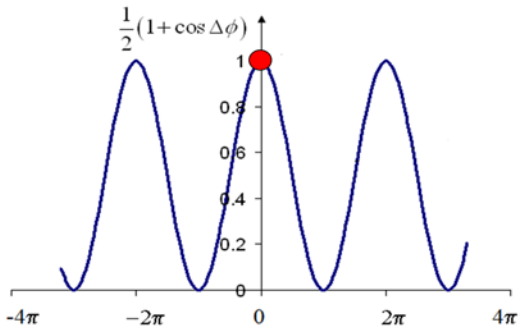

Figure 2-3 Interferogram at detector

In this figure we can see the detector output versus Sagnac phase shift $\Delta\phi$. When there is no rotation, $\Delta\phi = 0$, we will be at the point marked with the red dot. Any rotation will move the point in an amount proportional to $\Delta\phi$. As can be seen in the example from the previous section $\Delta\phi$ can be very small. So, there are obvious disadvantages to have this peak point as the operation point for a FOG.

These disadvantages are;

- **Low sensitivity:** As calculated in the example in the previous section.
- **No information on direction of rotation:** In case of rotation that causes some phase shift, in either case whether the rotation is clockwise or counterclockwise, we have a decrease in detector output. Therefore we are not able to detect the direction of this specific rotation.

However, the main purpose of a FOG is to measure rotations precisely with their direction. In this case we introduce the concept of bias modulation. This corresponds to adding a non-rotation-induced phase shift to the system [18].

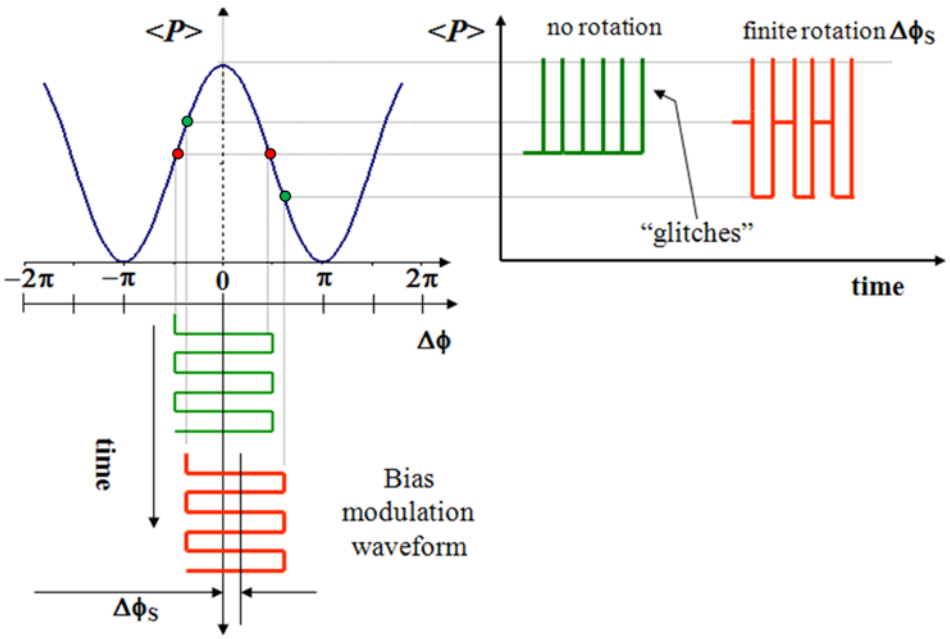

Figure 2-4 Square wave bias modulation[17]

This is achieved by placing a phase modulator (electro-optic or piezoelectric) at one end of the fiber coil [19]. Phase modulators will be explained in more detail in Chapter 3.

Examining Figure 2-4 clarifies the concept of square wave bias modulation. As it can be seen from the figure, instead of having the operating point at the peak of the detector signal (Figure 2-3), bias modulation shifts this point to -π/2 and + π/2 (points with the red dots on the interferogram).

The green graph at the upper right corner of Figure 2-4 shows the detector output in case of no rotation. Looking at the DC levels of this graph, one can see that they have the same value indicating that there is no rotation. On the other hand, the red graph shows the case where there is a finite rotation. DC levels of this graph differ about the modulation points of -π/2 and + π/2. This difference comes from the additional Sagnac phase shift due to rotation.

Obviously the difference in the two adjacent levels' value is proportional to the rotation rate of the loop.

2.2.3 Appropriate Modulation Frequency

One other very important aspect about bias modulation is to modulate the system at a proper frequency [20]. In order to switch the operation points to -π/2 and + π/2 appropriately, the modulation frequency has to be set so that both counter propagating beams do not pass the phase modulator at the same modulation level i.e. when the square wave is high (or low). This corresponds to biasing the phase modulator at

$$f = 1/(2\tau) \tag{2.14}$$

where f stands for the modulation frequency and τ is the loop transit time for the light beam.

To give an example consider a loop of length L=1000m and refractive index n=1.5. Therefore,

$$\tau = L/(c/n) = 1000/(3\times10^{8}/1.5)$$

Since c stands for speed of light, loop transit time for this system is $\tau = 5\times10^{-6}$ seconds. Substituting in (2.14) we get the appropriate square wave bias modulation frequency as,

$$f = 1/(2\tau) = 1/(2\times5\times10^{-6}) = 100kHz$$

2.3 Reciprocity

2.3.1 Principle of Reciprocity

Since the Sagnac effect results in a small phase shift which is to be detected, non-rotational, or in other words non-reciprocal phase shifts that occur because of environmental effects may suppress the Sagnac phase shift. In order to measure the Sagnac phase shift free from non-reciprocal phase shifts it is necessary to reduce these external effects. To fulfill this necessity counter propagating light

beams have to travel identical paths. In this case beams will be equally affected by environmental changes, resulting in no phase shift between counter propagating waves. The goal is to ensure that the Sagnac effect is the only source of non-reciprocal phase and is achieved by constructing the FOG system according to a reciprocal configuration [14].

In Figure 2-5, which represents a reciprocal FOG configuration, clockwise and counterclockwise optical paths can be seen to be identical. The clockwise wave passes twice beam splitter 2 to enter and exit the loop where it is the same for the counterclockwise wave. In addition, both waves pass through the phase modulator at the end of the coil.

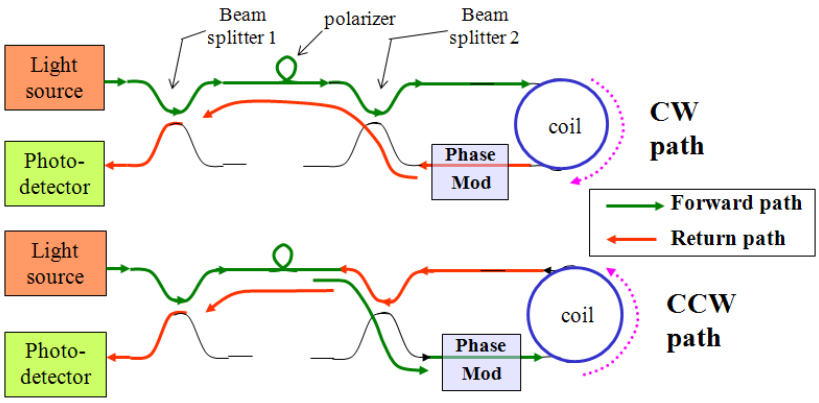

Figure 2-5 Reciprocal FOG configuration [17]

This can be clarified with a simple example. It is known that waves acquire 90 degree phase difference as they cross between coupler legs [21], such a reciprocal configuration ensures that both waves cross coupler legs an equal number of times so that there is no non-reciprocal phase shift between them. In addition to this, if the fiber medium is linear, time-invariant and free of magnetic fields the only phase difference that occurs between counter propagating waves is the Sagnac effect due to rotation of the fiber coil [21].

2.3.2 Problem of Polarization Non-Reciprocity

Single mode fibers propagate two orthogonal polarizations of the fundamental spatial mode. These two polarizations propagate at different velocities in the fiber since they have different propagation constants. Therefore after passing the (non-rotating) fiber loop, the two waves may not have the same phase. Moreover, imperfections within the fiber, external and winding stresses such as bending and twisting cause these polarizations to be cross coupled along the fiber. These errors, which create additional phase shifts between counter propagating waves is called the polarization non-reciprocity (PNR) of the fiber coil [22]. In order to reduce this PNR phase error a polarizer can be used as shown in Figure 2-6.

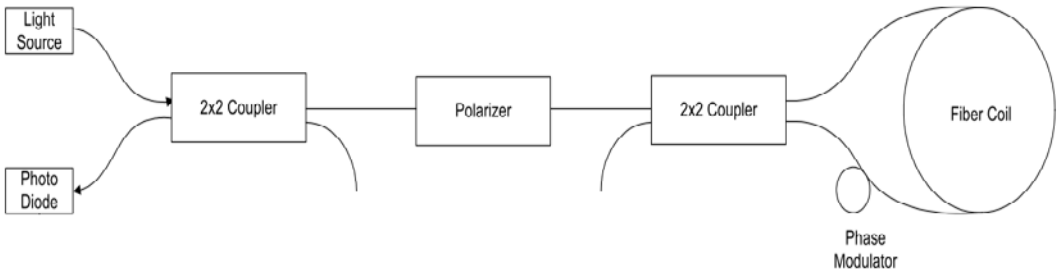

Figure 2-6 Reciprocal FOG configuration with polarizer

With this configuration (Figure 2-6) one polarization is chopped before the beams are split. The same applies at the end of the loop when waves recombine. This time, again the same polarization is chopped/filtered which was created during the propagation within the coil because of cross couplings of the polarization states [23].

In the late 1970's, with the developments in the telecom industry, polarization maintaining fibers (PMF) became available. These fibers (ideally) do propagate only one polarization. Although these fibers are comparatively more expensive, the use of PMF in FOG sensing coils minimizes the PNR error [22].

2.3.3 Use of a Depolarizer

The instability of the state of polarization in FOGs restricts the performance of the entire system. Besides preserving the state of polarization inside the fiber as explained in section 2.4.2 there is another way to overcome this problem. By using Lyot type fiber depolarizer not only are these effects on the performance of the FOG reduced the cost of the FOG is also decreased when low/medium performance FOG production is the case. In this method, instead of preserving the state of polarization, it is chosen to have a randomly distributed polarization that is evenly distributed over all possible states [24].

Lyot depolarizer, named after its discoverer Bernard Ferdinand Lyot, is a simple but efficient device which scrambles the input polarization, in other words, it converts polarized light into unpolarized light. Lyot, who was the first to demonstrate this invention used two wave plates with their fast axes 45^{o} apart, with the second plate twice the thickness of the first (Figure 2-7).

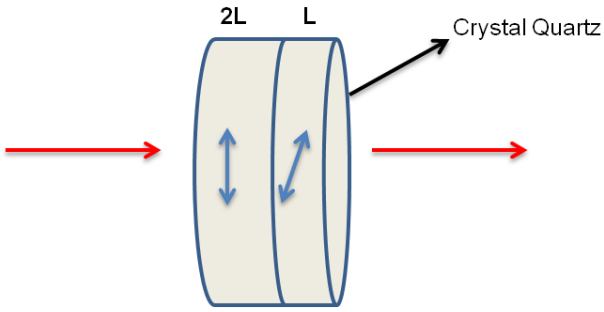

Figure 2-7 Lyot depolarizer (wave plate)

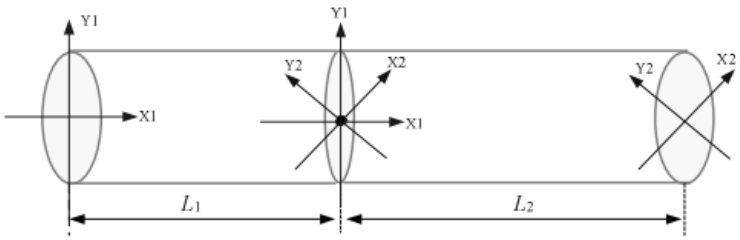

Figure 2-8 Lyot depolarizer (PMF)

Since FOGs are all fiber systems, the Lyot depolarizer shown in Figure 2-7 has to be converted into a fiber structure. This is achieved by using polarization-maintaining fibers instead of wave plates. The same principle applies with the PMFs. In order to create a Lyot depolarizer, two portions of PMF, with the second twice the length of the first, are spliced together with a splice angel of 45^{o} between their polarization maintaining axes (Figure 2-8). In doing so, the light is completely depolarized. The use of a Lyot depolarizer in a FOG setup will be further explained in Chapter 3.

CHAPTER 3

DESIGN OF A FOG

In this thesis we constructed a FOG system with SM fiber in the coil. The system is explained throughout the thesis. In this chapter, first, each component used in the FOG construction is explained with emphasis on the technical requirements for their use in the system Each component used in the system adds towards measuring a successful signal at the photodetector.

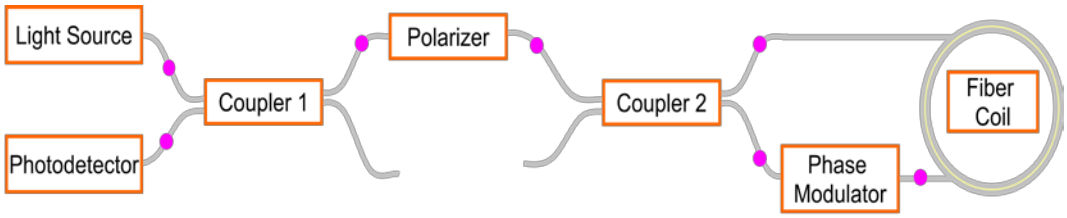

Figure 3-1 Minimum Reciprocal FOG configuration

3.1 Components of a FOG

In this section, a FOG system with minimum reciprocal configuration (Figure 3-1) is examined component by component. First, the light source with alternative approaches is discussed. The incoherent source is critical for successful operation of the FOG. Superluminescent Diodes (SLD) will be compared to Erbium(Er)-doped superfluorescent sources which was used here. Then, emphasis will be given on the couplers and polarizer, and their working principles will be discussed. Various types of electro-optic phase modulators used for modulation of the signal is analyzed. In this topic, an alternative approach to the phase modulator that becomes available with the use of a multifunctional

integrated optic chip (MIOC) will be examined as well. The MIOC houses the polarizer, phase modulator and second coupler on a single crystal, and enhances the FOG system by simplifying the configuration as well as the assembly. The sensing coil (fiber loop) and a special winding technique (called quadrupolar winding) is also examined. Finally, the detector is analyzed since it is integral in converting optical signals into electrical data.

3.1.1 Light Source

As most powerful optical systems require narrow bandwidth light sources such as lasers etc. it is critical for systems like FOGs to operate with broadband light sources [26]. The main reason to this requirement is to reduce the errors associated with coherence. One of the major error sources that FOGs suffer from is due to the Rayleigh backscattering. Optical fibers can attenuate light that is propagating within them by scattering it. Some portion of this backscattered light is sent along the fiber to the detector. Since this is the case for both counter propagating waves, there will be four waves incident on the detector; the two carrying rotation information and the other two carrying just noise due to this backscattering. Considering that this happens all over the fiber length that can be thousands of meters, this noise, can be in the order of several degrees per seconds. Therefore, this error source has to be eliminated in some way [22]. The most efficient way to eliminate this error source is to use broadband light sources which have short coherence lengths.

In order to construct a good quality FOG one has to start by constructing a good quality light source. Key parameters to such a light source can be summarized as the following:

- **Broadband Light:** Light sources used for FOGs should have a broad spectrum in order to reduce errors due to backscattering as explained above.
- **Adequate Power:** Light sources should be able to produce enough power that can be efficiently coupled into a single-mode fiber.
- **Wavelength Stability:** Light sources used in FOGs should have good wavelength stability over time and temperature. As explained and

calculated in 2.1.2 wavelength (frequency) stability is directly proportional to scale factor stability that is one of the key parameters for FOG performance.

- **Long Lifetime:** FOGs stand for long lifetime/reliable rate sensors, therefore their light sources should also meet this requirement.

Table 3-1, adopted from [26], lists the requirements of light source parameters in order to have a good quality FOG, along with motivations to meet these requirements and goals aimed.

Table 3-1 Light source requirements for FOG

Requirement	Motivation	Goal
Broad spectral width.	Elimination of coherence errors due to 1) Rayleigh backscattering 2)Polarization cross-coupling	At least 5nm (the more the better)
High power in single mode fiber.	Improved signal to noise ratio (SNR).	10mW (depends on application)
Mean wavelength stability.	Stable FOG scale factor.	<10ppm (depends on application)
Long lifetime	Reliability.	Longer than available sources
UV radiation sensitivity	Operation in adverse environments.	long wavelength operation >1.3μm

3.1.1.1 Superluminescent Diode

The invention of the Superluminescent diode light sources (SLD or SLED) in 1986 was the first step in eliminating this error. SLDs usually have a coherence length of 50 to 100μm, which is very small compared to the length of the fiber used in the FOGs. Because of their broadband spectrum and small size, SLDs have been the choice for FOG applications after their invention [28]. SLDs, as other broadband light sources, do not reduce the amount of backscattered light power

that reaches the detector, they only reduce the backscattered light that coherently adds to the main signal that contains information on rotation [24].

Despite the fact that SLDs meet most of the requirements listed in Table 3-1 they lack mean wavelength stability under varying temperatures. Most SLDs exhibit a wavelength/temperature dependence of 400ppm/Cº. In this case, if one wants to construct a light source for a navigation grade FOG (1ppm/ºC) using such an SLD, temperature control of the SLD at a level of 0.0025ºC will be necessary. Moreover, light emitted by an SLD cannot be efficiently coupled into a fiber, thus decreasing the power fed to the optical system [29]. Because of the reasons explained above SLDs are not the primary choices for FOGs when precision detection of low rotation rates is necessary.

3.1.1.2 Erbium Doped Superfluorescent Fiber Sources (SFS)

Light source requirements in order to construct a working FOG are described in section 3.1.1. Another alternative to the SLD, the erbium doped superfluorescent fiber source (SFS), is the premium choice for FOG applications [29].

Erbium (Er) doped SFS are light sources that exhibit amplified spontaneous emission (ASE). Instead of using the diode as the light source as in SLDs, a powerful laser diode is used to pump a gain medium to obtain the ASE. Then the amplified spontaneous emission of the gain medium serves as the light source to the FOG. Therefore, these SFS sources are sometimes called ASE sources. The working principle of this light source is to use a pumping source to excite a gain medium, which is Er-doped fiber in this case. Then the excited medium emits the desired light that will be circulated within the FOG.

With careful selection of the source configuration, pump wavelength, pump power, fiber length and fiber concentration/composition all requirements that is necessary for a FOG can be met [30].

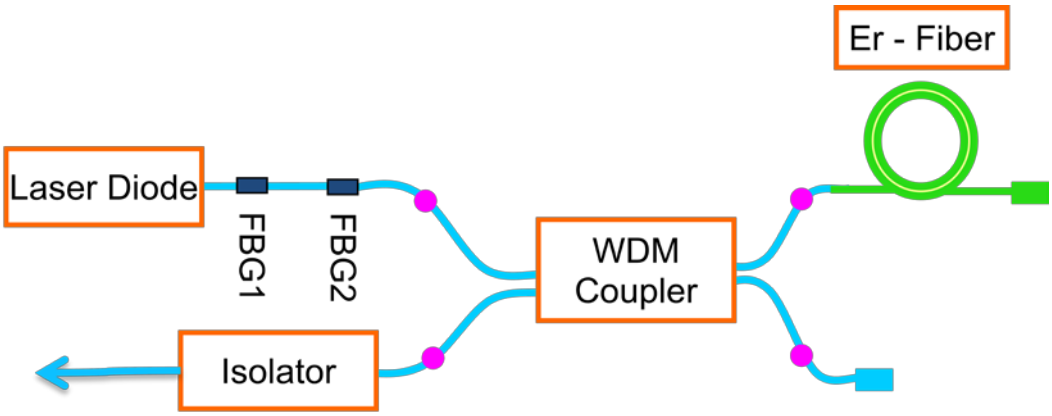

Figure 3-2 Erbium doped superfluorescent fiber source (SFS) configuration

According to [29], we have constructed the above configuration (Figure 3-2) as our light source for the FOG designed and analyzed in this thesis. Design parameters of the constructed light source are listed in Table 3-2.

Table 3-2 Light source design parameters

Pump Source / Wavelength	Uncooled pump laser module	980nm
Pump Power	@250mA	120mW
Gain Fiber	Erbium Fiber	1.5m

Using this configuration, we get an output close to 10mW of ASE at 1550nm when the pump is biased at 250mA drive current. Considering that most SLD's at this biasing current emit an output of 500µW up to 1mW, it is more advantageous to use an SFS due to increase in the signal to noise ratio (SNR).

Moreover, with the use of fiber Bragg gratings at the output of 970-980nm pump diode the wavelength of the pump source is kept constant as much as possible. The datasheet of the pump source we used indicates that the value $d\lambda/dT$ is

0.02nm/ ºC. This corresponds to 20ppm/ºC. In section 3.1.1.1 it was stated that most SLD's have wavelength temperature dependence in the range of 400ppm/ºC.

In summary, requirements of the light source used with a FOG such as high output power, broad emission bandwidth and excellent spectral thermal stability are met with design parameters listed in Table 3-2.
Optical spectrum analysis of the different spectra we have within the SFS light source will shown in section 3.2.2.

3.1.2 2x2 Coupler

Unlike the Er-doped SFS, which is a combination of various components, the fiber optic coupler (Figure 3-3) is a single element in the FOG system.

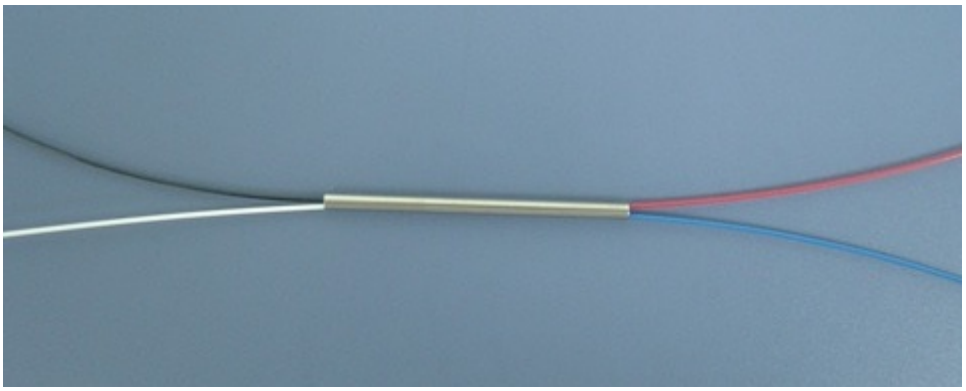

Figure 3-3 Fiber Optic 2x2 Coupler

A coupler's main purpose is to direct and split light. Even though each fiber attached to the coupler is considered as an input or an output, as in Figure 3-3 manufacturers usually prefer to color the fibers. Black is used for input, while blue and red fibers are used for outputs. This helps identifying fibers going in and out a coupler when the coupler is used in a system. As it can be seen from Figure 3-4 which represents the FOG configuration, there are two couplers used within the system.

The first coupler is used to direct light from the light source to the gyro loop in forward path and direct light back to the photodetector in backward path. The

second coupler is used to split light equally (50/50 or 3dB) at the entrance of the fiber coil and combine the returning lights in backward path.

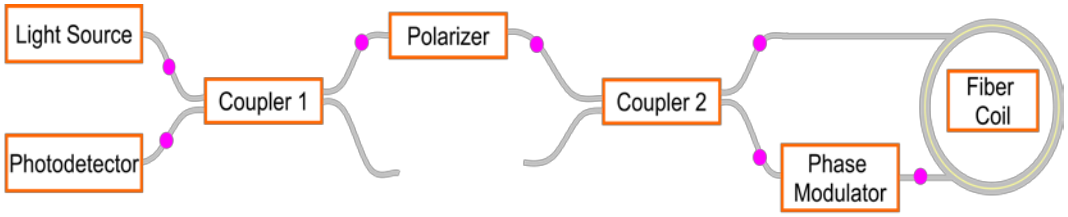

Figure 3-4 FOG Configuration

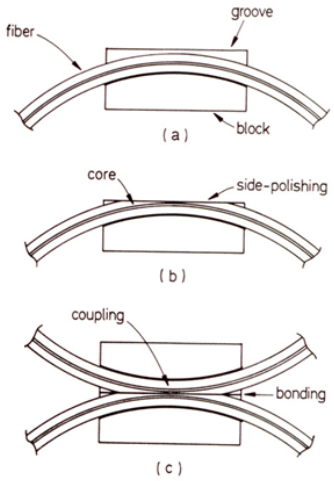

Figure 3-5 Side polishing technique [31]

To get a 3-dB coupler a design parameter called coupling strength has to be adjusted very well, this is done by adjusting the core-to-core distance. An efficient method in fabricating such a coupler is the side polishing technique [8]. In order to have a basic idea about how such couplers are fabricated, the side polishing technique can be simply explained as follows; As in Figure 3-5, a fiber is bonded into a silica block (Figure 3-5 a). The block is polished to remove the cladding as in Figure 3-5 b. Finally two identical blocks are brought together with an index-matching fluid. The shiny outer surface in Figure 3-3 is the housing that protects the coupler from outer effects.

Different types of fibers such as polarization maintaining fibers can be used to produce a coupler. In this case, the coupler will preserve the polarization of the input light as well. However, care must be taken with the alignment of the polarization preserving stress rods within the PMF [31].

3.1.3 Polarizer

The management of polarization is a crucial task in telecommunication, interferometric sensors and especially in FOGs. In order to make accurate measurements it is essential to have light in one polarization [32]. As mentioned before in this thesis the major way of eliminating the polarization non-reciprocity error is to use a polarizer [23]. Another requirement that makes the use of a polarizer essential, is the need for linearly polarized light when modulating the phase of light waves with an electro-optic phase modulator [8].

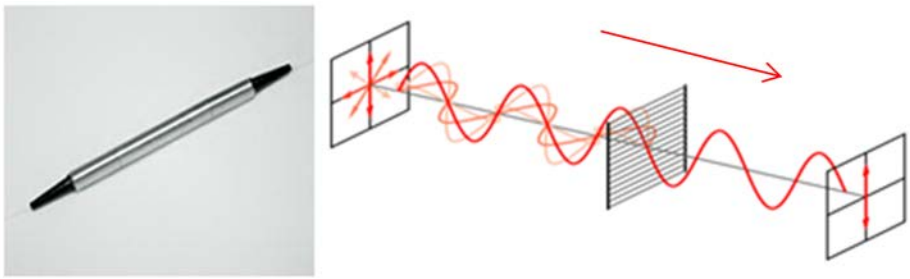

Figure 3-6 Fiber-optic polarizer and linear polarization

A polarizer simply filters unpolarized light allowing light at one single polarization to pass through the output (Figure 3-6).

As it can be seen in Figure 3-6 a polarizer looks quite similar to a coupler from the outside. However, it has a single fiber input and a single fiber output. Since the output light waves will be linearly polarized, the fiber at the output is PMF.

There are several ways to polarize light waves. Bulk optics elements could be inserted into FOG systems, however considering many disadvantages of it such

as coupling losses, size and cost considerations, mechanical and thermal stability issues etc. using in-line fiber-optic polarizers would be the best choice [33].

There are many techniques to design and produce in-line fiber-optic polarizers. One way of producing such polarizers is to use the side-polishing technique [34]. To have a basic idea about how in-line fiber-optic polarizers are manufactured side-polishing can be simply explained as follows. In this technique, a portion of the fiber cladding is polished away. Instead of the removed cladding, a thin metal film (gold or silver) is deposited onto this polished region by vapor deposition. This overlay of thin metal film acts as a multimode slab waveguide coupled to the optical fiber. Light in the fiber interacts with TE and TM modes of the overlay at different wavelengths. This design (Figure 3-7) serves as a polarizer [35]. Most polarizers on the market today have a polarization extinction ratio (PER) above 30dB. Measurements of PER will be covered in section 4.1.4.

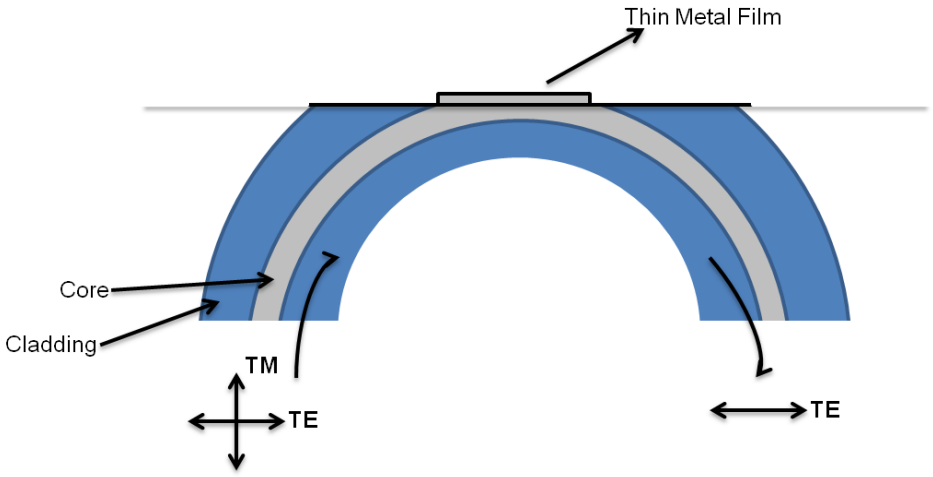

Figure 3-7 Schematic of the fiber polarizer

3.1.4 Electro-Optic Phase Modulator

As explained in previous chapters, bias modulation, or modulating the FOG at proper frequency and the necessity of a reciprocal configuration forms the primary requirements for the operation of the FOG. The so-called "heart of the FOG" which is the phase modulator is involved to satisfy all these requirements.

Electro-optic modulators are signal-controlled devices that demonstrate electro-optic effect therefore, they modulate beam of light passing through it. These modulators may impose modulation on the frequency, phase, amplitude or polarization of the light beam [36].

Considering the FOG, we will be dealing with the phase modulator type of these modulators. Simplest and most efficient way to do so is to use a crystal such as lithium niobate ($LiNbO_3$) which shows change in refractive index when exposed to an electric field [37]. This phenomena (electro-optic effect also called as Pockels effect) is achieved by placing a parallel plate capacitor along the crystal and forming a waveguide between the plates of the capacitor (Figure 3-8), which is possible by various manufacturing techniques. These techniques are described and discussed in the next section.

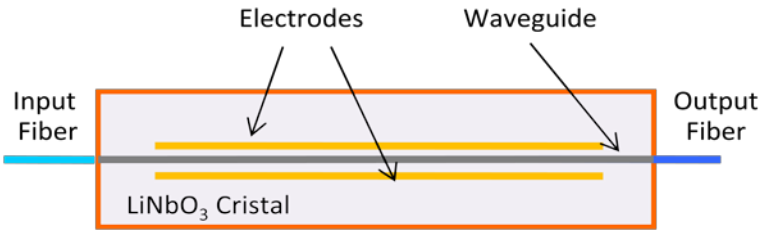

Figure 3-8 Basic phase modulator design on $LiNbO_3$ crystal

As in Figure 3-8 the basic element of the phase modulator is the waveguide. This waveguide is formed by increasing the refractive index of the $LiNbO_3$ crystal by doping it using microlithography technology. As the dopant material, which is titanium, diffuses into the crystal it increases the refractive index of the crystal just underneath the surface. The surroundings to this doped region then acts just as the same as cladding acts in a fiber-optic cable. By proper selection of dopant concentration, width and depth, cladding to core refractive index differences of an optical fiber is achieved between the crystal and the waveguide on it. To couple light into the waveguide edges of the crystal are polished and connecting fibers are attached to the crystal by means of butt coupling.

As discussed previously, waveguides on $LiNbO_3$ crystal are usually fabricated with the titanium (Ti) indiffusion technique. By means of lithographic masking very narrow strips of thin film titanium are deposited onto the crystal, then by heating the crystal up to 900°C to 1100°C for a few hours, the deposited Ti diffuses into the crystal increasing the refractive index forming the waveguide (Figure 3-9) [38].

Figure 3-9 Fabricating waveguides on $LiNbO_3$ by titanium indiffusion

The electro-optic effect has been utilized extensively for various applications in optoelectronics. Anisotropic or isotropic crystals can be used to observe this effect when an electric field is applied. For modulation purposes the crystal has to be chosen so that it is mostly transparent to wavelength of interest and also that when an electric field is applied the desired change in the phase of the beam is seen for an appropriate thickness and bias voltage. $LiNbO_3$ is ideally suited for applications at 1550nm. The $LiNbO_3$ crystal is a uniaxial birefringent crystal with linear electro optic effect coefficients determined by its second order non-linear susceptibility [39]. Different orientations of the driving electric field between the capacitor plates ($\mathbf{E}_d$) and optical electric field ($\mathbf{E}_o$) that is passing through the waveguide will result in different changes in the refractive index of the crystal. The $LiNbO_3$ crystal has symmetry of 3m. The electro-optic coefficient matrix according to Yariv [40] is as follows:

$$r_{ij=}\begin{bmatrix} 0 & -r_{22} & r_{13} \\ 0 & r_{22} & r_{13} \\ 0 & 0 & r_{33} \\ 0 & r_{51} & 0 \\ r_{51} & 0 & 0 \\ -r_{22} & 0 & 0 \end{bmatrix} \tag{3.1}$$

Where r_{13}=8.6 pm/V, r_{22}=3.4 pm/V, r_{33}=30.8 pm/V and r_{51}=28 pm/V.

In order to get the strongest change in refractive index for $LiNbO_3$ crystal, the r_{33} (r_{33}=31 x 10^{-12}m/V) term has to be used. This means that $\mathbf{E}_d$ and $\mathbf{E}_o$ has to be parallel to the extraordinary z-axis of the crystal. The change in refractive index in such a configuration then is given as in equation (3.2).

$$\delta n_z = -\frac{1}{2} n_z{}^3 r_{33} E_{dz} \tag{3.2}$$

In this equation δn_z stands for the change in refractive index along the z-axis of the crystal and E_{dz} is the electric field component along z-axis of $\mathbf{E}_d$. To have a better understanding on this concept, two of the probable different orientations can be seen in Figure 3-10.

In this case, it is necessary that linearly polarized light has to be entered into the waveguide in order to achieve a good performance out of the phase modulator. Furthermore, since the $LiNbO_3$ crystal acts different to the light beam along each axis, the $LiNbO_3$ crystal to used to fabricate a phase modulator has to be properly cut.

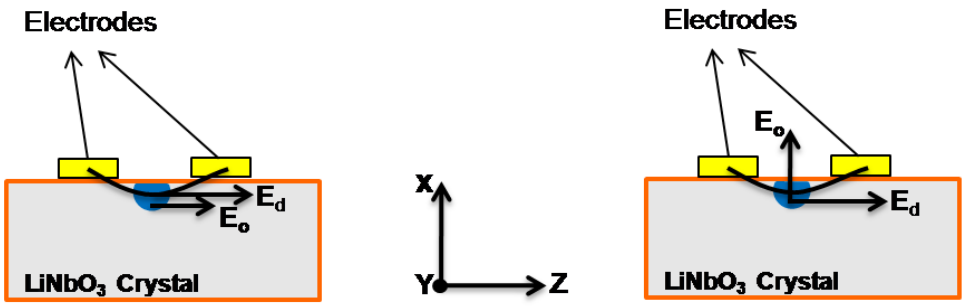

Figure 3-10 Light beams with different polarization states entering an x-cut y-propagating phase modulator

As explained before, we get the strongest electro-optic Pockels effect if the r_{33} coefficient is used, that is, if the phase modulator configuration is designed as it is in the left-hand side of Figure 3-10. This configuration is called "x-cut y-propagation", where the waveguide is parallel to the y-axis of the uniaxial birefringent $LiNbO_3$ crystal and the x-axis is perpendicular to the substrate surface. Again, input light polarization has to be aligned according to Figure 3-10 as well.

Just to have an idea of how entering a light beam with a different state of polarization would affect the strength of the electro-optic Pockels effect, we can check the electro-optic coefficient r_{13} (9 x 10^{-12} m/V) that applies if the right-hand side configuration in Figure 3-10 is used. In this case (remembering that r_{33}=31 x 10^{-12}m/V), if someone wants to fabricate a phase modulator using the r_{13} coefficient, he has to make the modulator more than three times longer than it would be with the suggested r_{33} coefficient in order to obtain the same strength of phase modulation [41].

$$\delta\Phi = 2\pi\delta nL / \lambda \tag{3.3}$$

Equation (3.3) explains how much phase difference is in a phase modulator with wavelength of light (λ) that is propagating through the phase modulator of length

L. Where δn is calculated in equation(3.2). Replacing E_{dz} in equation (3.2) with $\frac{V}{d}$ for the electric field between the capacitor plates, where V is the applied voltage and d is the distance between the plates of the parallel plate capacitor, a critical parameter for the phase modulator comes up. This parameter is V_π, which describes how much voltage has to be applied to achieve a phase modulation of π radians to the light beam. Substituting equation (3.2) into equation (3.3) and inserting value π instead of $\delta\Phi$ we get the V_π value for an x cut y propagation crystal with light beam propagating through it with TE mode polarization as follows [36]:

$$V_\pi = \frac{d\lambda}{n_z^3 r_{33} L} \tag{3.4}$$

From equation (3.4) it is obvious that V_π increases with wavelength and decreases with modulator length. To have an idea of V_π values of modulators with different configurations, Table 3-3 can be examined.

Table 3-3 V_π values for different phase modulator configurations

Modulator Length	Wavelength	Cristal Configuration	Input Light Polarization	Electro-Optic Coefficient	V_π
10 cm	850 nm	x-cut, y-prop.	TE	r_{33}=31 pm/V	**2.0 V**
10 cm	1300 nm	x-cut, y-prop.	TE	r_{33}=31 pm/V	**4.5 V**
10 cm	1550 nm	x-cut, y-prop.	TE	r_{33}=31 pm/V	**5.4 V**
10 cm	850 nm	x-cut, y-prop.	TM	r_{13}=9 pm/V	**7.0 V**

3.1.5 Multifunctional Integrated Optic Chip (MIOC)

Although Ti-indiffusion waveguides is a very suitable technique for fabricating waveguides on a crystal, a waveguide that permits the propagation of a single waveguide would be much more preferable in a FOG system. Such a waveguide fabrication, instead of Ti-indiffusion, can be achieved by the proton exchange

method. In this method the $LiNbO_3$ substrate is placed in a melted organic acid where the proton exchange happens. H^+ ions from the melted organic acid replace Li^+ ions in the crystal lattice. This technique has a very important result; as it increases the refractive index of the low extraordinary axis, it decreases the high refractive index of the ordinary axis. This course of action results in a waveguide that guides only z-polarized mode of light parallel to the extraordinary axis. Very high polarization extinction ratios are obtained in this way [42].

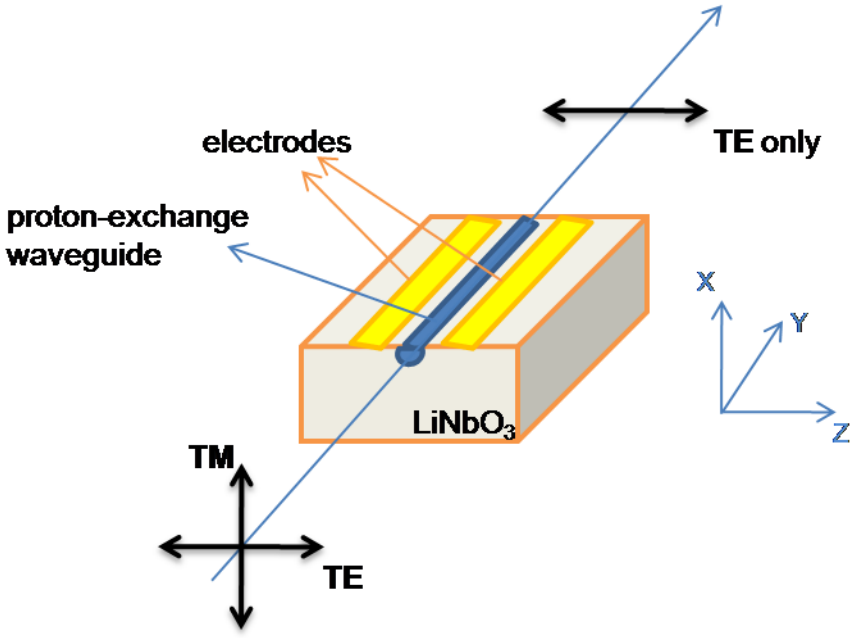

Figure 3-11 Single polarization propagation through a proton exchange waveguide

Figure 3-11 clarifies the benefits of waveguides fabricated by proton-exchange technique. As in Ti-indiffusion, the strongest electro-optic coefficient is obtained with the x-cut y-propagation crystal. Nevertheless, this time, even a single mode fiber that permits all polarization states to be propagated, can be butt coupled to the entrance of the crystal. This will not affect the quality of phase modulation, as it is not the case with Ti-indiffusion waveguides. In order to use the r_{33} coefficient of the electro-optic effect with $LiNbO_3$ crystal light polarized in the z-axis has to be input into the crystal when using Ti-indiffusion waveguides.

Even though this type of phase modulator also serves as a polarizer, this configuration still does not allow the removal of the polarizer necessary for the operation of the FOG (Figure 3-4). If we remove the polarizer with this configuration, light wave passing coupler 2 from the arm without the phase modulator will not be polarized . However, if we use a phase modulator where the waveguide is fabricated by the proton-exchange method, light beam passing through the lower branch with the phase modulator will be polarized. This inconsistency will cause the PNR to grow significantly.

With the development of the proton exchange waveguide modulator, one can incorporate the second coupler to within the entire structure reducing the complexity of the FOG system. This is done fabricating the multifunctional integrated optic chip (MIOC). The MIOC, which is quite consistent with its name contains three components on a single crystal.

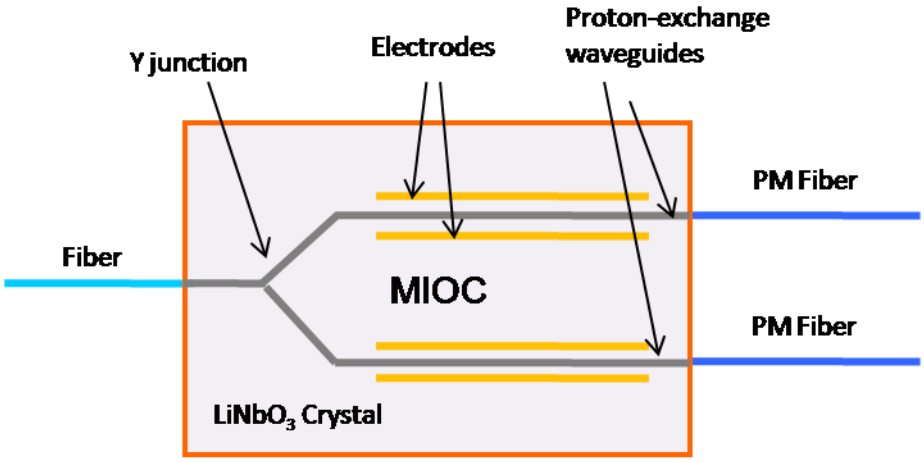

Figure 3-12 The multifunctional integrated optic chip (MIOC)

Figure 3-12 shows all these three components. The y-junction is fabricated by masking techniques so that the waveguide forms a splitter with 3dB splitting ratio in the forward direction and a combiner at the backward direction for the light. There is no longer any need for a polarizer before the second coupler in the FOG configuration since the waveguide itself is a polarizer. Consequently, electrodes placed at both arms serve as phase modulators. This innovation has brought a great simplicity in FOG design where it reduces size and cost of the FOG [43].

This remarkable simplicity can be seen in Figure 3-13(b) where Figure 3-13(a) is the more complicated conventional minimum reciprocal configuration of the FOG.

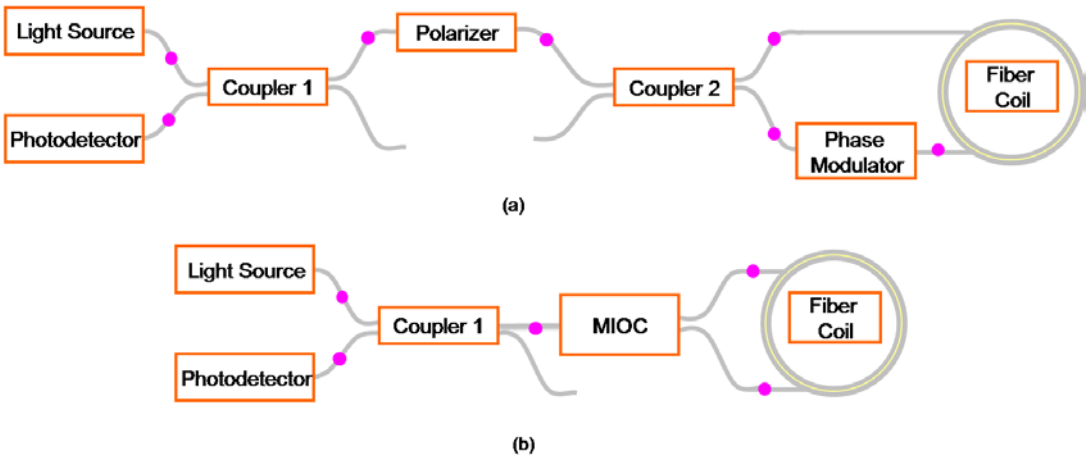

Figure 3-13 FOG configurations (a) with conventional phase modulator (b) with MIOC

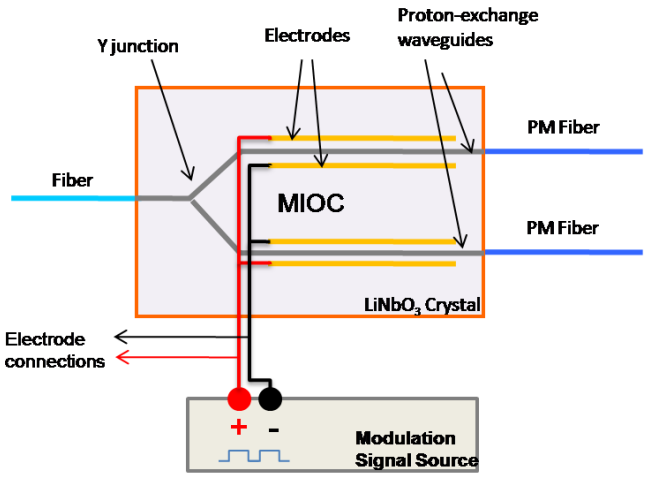

Figure 3-14 Push-pull phase modulation

Investigating Figure 3-12 we see that both branches of the y-coupler have electrodes along with the waveguides. The reason for this is the advantageous push-pull modulation technique.

Figure 3-14 is a demonstration of the push-modulation technique. In this way as a negative phase is added to the upper arm of the modulator, a positive phase is added to the lower arm. By doing so, for the same modulator length as with conventional phase modulators, the V_π parameter discussed in previous section is reduced by a factor of two [44].

The next topic is the fiber coil which is the sensing element for the Sagnac effect.

3.1.6 Fiber Coil

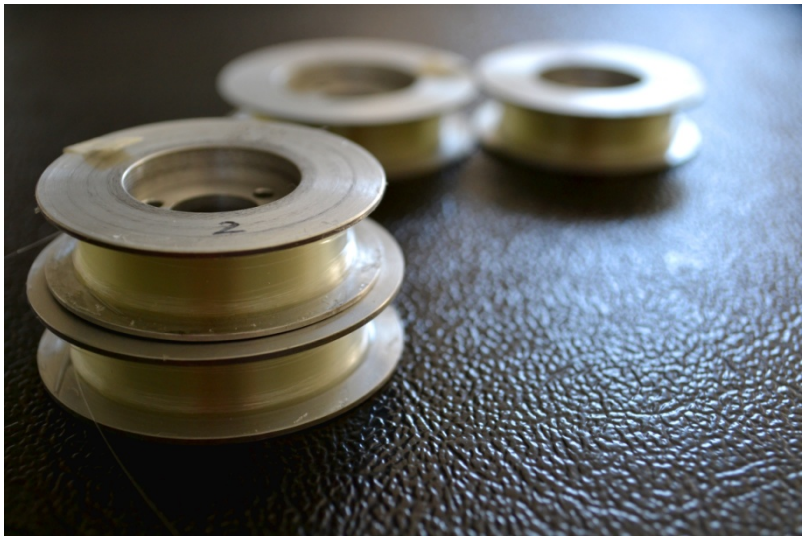

Figure 3-15 200m PMF fibers on 25mm and 30mm inner diameter coils

As explained in 2.1.2 the Sagnac effect is closely related with the fiber coil parameters of the FOG. Remembering equation (2.10);

$$\Delta\phi_{Sagnac} = \frac{2\pi LD}{\lambda c}\Omega$$

values L (length of the fiber coil) and D (diameter around which the fiber is wound) determine the resultant Sagnac phase shift due to some rotation Ω. Simplifying this; L and D when used with a certain wavelength (λ) of light determine the scale factor (equation(2.11)). Which describes how much phase shift will be generated

for a certain rotation Ω. Therefore, fiber coil parameters have to be chosen according to the requirements of the rotation to be measured. Usually, 200m fiber coils wound around a few cm of diameter (Figure 3-15) are used for tactical grade (<1°/h sensitivity) FOGs. 1000m of fiber wound around a diameter around 10cm is preferred when navigation grade (<0.01°/h sensitivity) FOGs are to be produced.

Different types of fibers can be wound around the coil. These fibers can be either PMF or non-PMF. However, the best performance out of a FOG is obtained when stress-induced high-birefringence polarization-preserving (maintaining) fiber is used as the fiber coil.

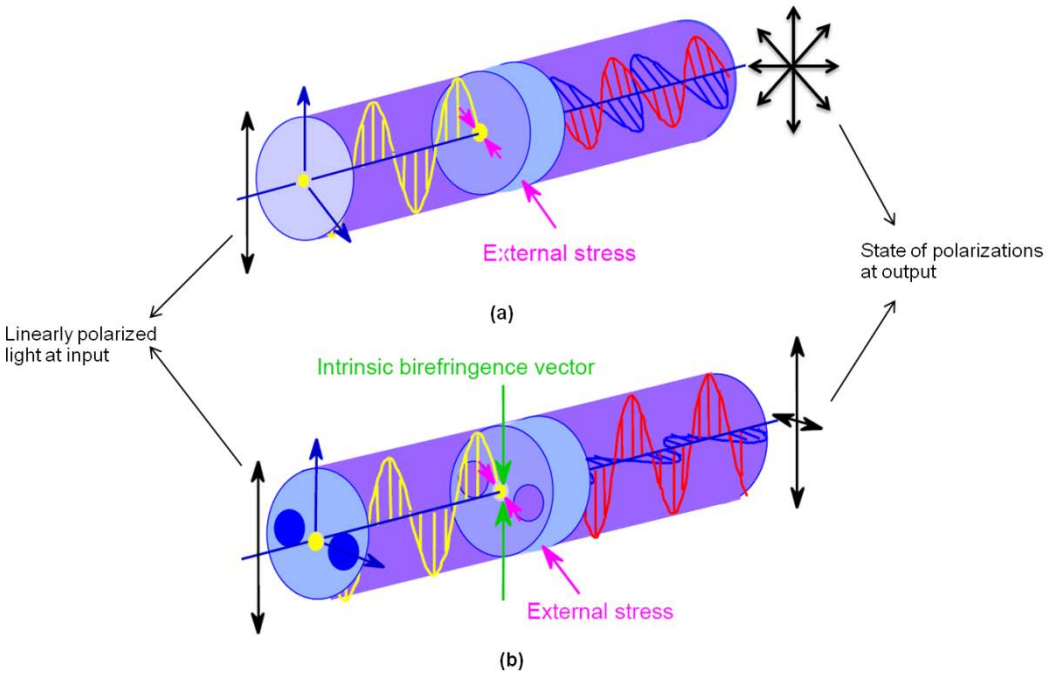

Figure 3-16 Propagation of linearly polarized light through (a) single mode fiber (b) single mode polarization maintaining fiber [17]

As explained previously, polarization cross-couplings within the fiber coil due to external effects such as stress and change in temperature results in the polarization non-reciprocity error. Figure 3-16 demonstrates the advantage of using PMF in order to reduce this error. In Figure 3-16(a) we can see how propagation of a linearly polarized light through a single mode fiber is affected due

to an external stress. Linearly polarized light beam will continue its propagation as randomly polarized (unpolarized) light after stress is applied to the fiber. However, this is not the case with PMF (Figure 3-16(b)). Due to the intrinsic birefringence vector created by the stress rods in this type of fiber the polarization of propagating light is almost well conserved [45]. However, the use of a Lyot depolarizer, discussed in previous sections, with non-PMF in the coil reduces this error [46].

Apart from the type of fiber used in the coil, there are other error sources to be considered in order to have a good quality fiber coil. One of these error sources is the Shupe effect. Shupe, et al [47] noticed that thermal gradients across the fiber coil create bias errors. Shupe error is due to the rate of change of the temperature of the fiber coil. This error is eliminated by winding the fiber symmetrically about the midpoint of the fiber. With such a winding, if the rate of change of the coil is symmetric then this error vanishes [48]. All modern FOGs have to use such winding patterns for the fiber coil. The quadrupolar winding technique gives the best performance in eliminating such errors [49].

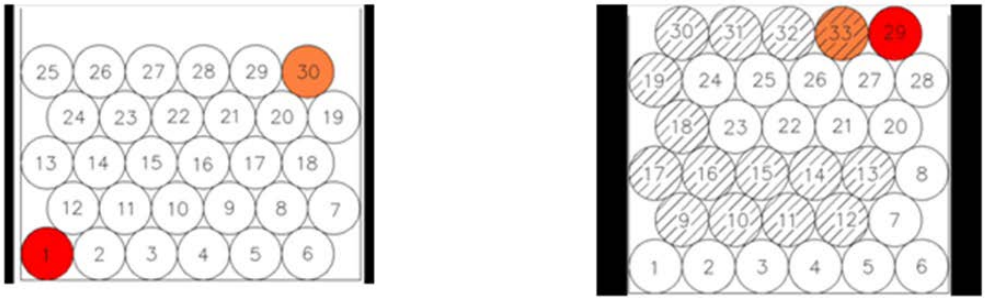

Figure 3-17 Cross section of (a) helical (b) quadrupolar wound fiber coils

Figure 3-17 is a representation of different fiber winding methods. Figure 3-17(a) represents the helical winding method. With this method, one end of the fiber is taken and wound around the coil until all the fiber is wrapped around the coil. This case is obviously not symmetric, that is, considering that there is a thermal gradient across the fiber coil, the red circle indicating one end of the fiber and the orange circle indicating the other end will have different temperatures. This will

cause counter propagating waves to acquire a non-reciprocal phase difference, creating an offset (bias) at the output of the gyro. This is not the case with a fiber coil wound by the quadrupolar winding method. As it shown in Figure 3-17(b), when the quadrupolar winding method is used both ends of the fiber lay side by side at the same level, as it is the case for all equidistant parts about the midpoint of the fiber. Dashed circles represent layers formed with fiber at one side of the midpoint where empty circles stand for layers of fiber around the coil, formed with fiber the other side from the midpoint of the fiber.

Another important but easy to solve error regarding the fiber coil is the Faraday bias error. The electromagnetic sensitivity of light propagating through a fiber is responsible for this error. A linear state of polarization is introduced into a fiber loop and this state of polarization rotates through an angle which is dependent upon the line integral of the magnetic field along the propagation path around the loop. Shielding the gyro coil with high permeability metals eliminates this error [50][51].

3.1.7 Detector

After having explained all optical components to design a FOG, finally it is important to work with the correct detector to detect the Sagnac phase shift. Wrong choice of a detector will degrade the performance of the FOG. Using the correct detector, the errors are by the shot noise [52]. Photon shot noise, which is due to the quantum nature of light, is the standard deviation of the rate of arrival of photons to the detector. A very nice numerical explanation on the theoretical limit for FOGs due to the photon shot noise is explained by Bergh, et al [14].

Semiconductor PIN photodiodes (Figure 3-18) have very high quantum efficiency, that is, the number of primary electrons generated is very close to the number of input photons and the flow of electrons has about the same shot noise as the theoretical value for the flow of photons [8]. Therefore, they are the primary choice as detectors for FOGs.

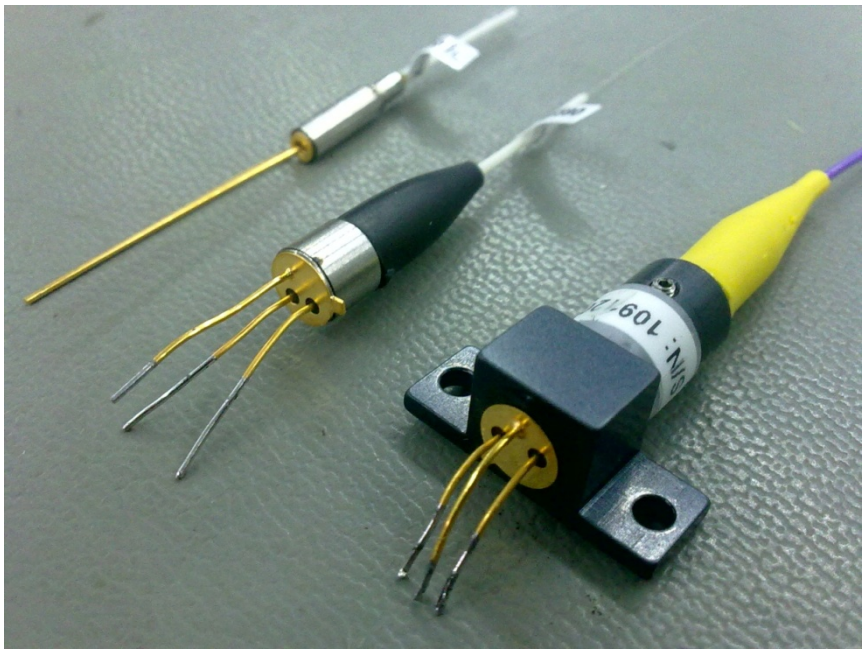

Figure 3-18 Three different brand InGaAs PIN Photodiodes (fiber pigtailed)

Since most FOGs operate at 850nm, 1300nm or 1550nm, PIN photodiode semiconductors have to be chosen accordingly. For 850nm, a Silicon (Si) photodiode is used. Indium Gallium Arsenide (InGaAs) is the semiconductor used in the case for 1300nm and 1550nm.

CHAPTER 4

ASSEMBLING AND TEST OF A FIBER-OPTIC GYROSCOPE

In this chapter the main focus is the design and measurement of a FOG in the Optoelectronics laboratory of the Physics Department located at Middle East Technical University, Ankara, Turkey. Initially splicing of optical fibers is explained. Then, all components are spliced together to form a FOG optical system. During these procedures, verification of datasheet values of components are done by means of optical loss measurements, optical spectrum analyzer measurements, optical time domain reflectometry measurements and polarization extinction ratio measurements. How these measurements are made, along with which devices are explained according to the outline of this thesis.

Furthermore, an electronic circuit, the transimpedance amplifier, which converts current generated within the detector to voltage, is also explained.

To summarize our test procedure, initially the FOG is tested by characterizing the phase modulator that was used in the system. After obtaining the correct V_{π} voltage for the electro-optic phase modulator a rotation table was used to make measurements with the FOG sensing coil rotating on the platform at known rotation rates. Finally, using these values, the scale factor for the FOG that was constructed is calculated.

4.1 Assembling and Verification

In this section, the assembly of the FOG system is explained. Components that are used (Figure 3-4) are listed in Table 4-1.

Table 4-1 List of components used

Component
Laser Diode
WDM Coupler
Erbium Fiber
Isolator
2x2 SMF Coupler
Polarizer
2x2 PM Coupler
Phase Modulator

4.1.1 Fiber Splicing

Fiber splicing also called fusion splicing is the act of joining two fibers end to end by using heat. Splicing is done in such a way that light passing a splice point between two fibers should not be scattered or reflected back. Moreover one other important necessity of a good splice is that the splice point should not be weak compared to the other parts of the fiber. In this way fiber-optic systems are assembled by splicing together fiber-optic components.

In practice, in order to make a good splice we can divide the splicing process into two parts. First is the preparation of fibers to be spliced and the second is the splice operation. Let us start with the first part; In order to prepare fibers so that they can be spliced together meeting the requirements of a good splice, the following in order has to be done:

- Stripping
- Cleaning
- Cleaving

In order to do these there are necessary tools. These tools are shown in Figure 4-2. First, let us examine the structure of a single mode fiber-optic cable (Figure 4-1).

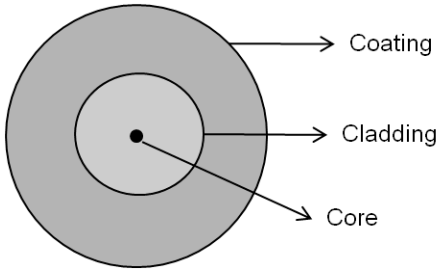

Figure 4-1 Single mode fiber structure

There is the core with the highest refractive index, surrounded with the cladding that has a lower refractive index compared to the core. Propagation of light is possible with these two layers. The layer outside these two is the coating that protects the fiber from outer effects. Since the core and the cladding are the layers that related with light propagation, fusion splicing of two fiber ends has to be among these two. Therefore, the coating must be stripped away. A stripper as in Figure 4-2 is required to do this.

Figure 4-2 Tools necessary to prepare fibers for splicing

Most single mode fibers have a cladding of 125µm in diameter and a coating of 250µm in diameter. This mechanic stripper must strip away the outer layer starting from 125µm up to 250µm. After stripping away the coating, the fiber is cleaned with alcohol to get rid of the residual particles on the coating that are left after stripping. A cleaning cloth that does not damage the fiber cladding is used to do this. If the fiber is not cleaned after stripping, dust particles will create defects during the splice operation, reducing the quality of the fiber splice. Stripping 2cm of coating away from both fiber ends will be enough. After having stripped and cleaned the fiber ends, it is time to cleave the fiber ends. We used the CT-30 cleaver from Fujikura to perform this task. A cleaver is a device on which the stripped part of the fiber is aligned perpendicular to a blade on the cleaver. The cleaving is achieved by first placing the fiber into a fiber groove on the cleaver and then the upper arm of the cleaver is pressed which mechanically releases a very fine blade that cleaves the fiber at a precise angle. The cleaving is so precise that the result is a surface perpendicular to the fiber axis that does not deviate more than 0.1 º.

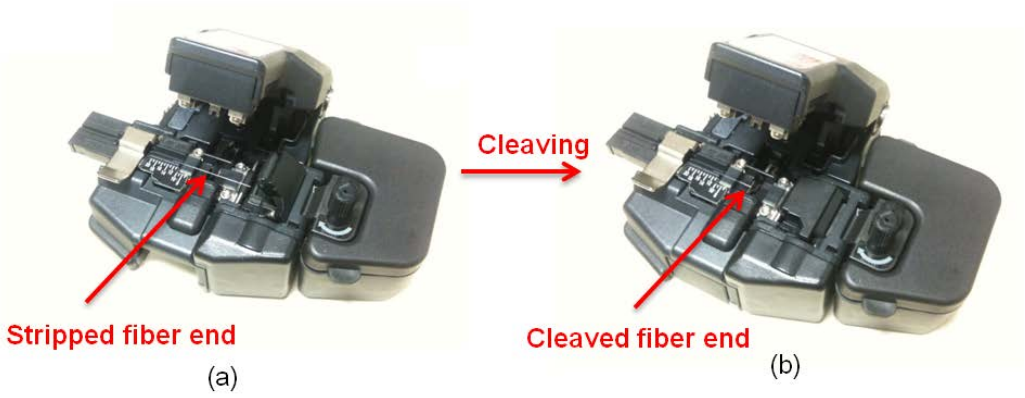

Figure 4-3 Cleaving of a stripped fiber (a) before and (b) after

To have a visual understanding of how to cleave a fiber, Figure 4-3 can be examined. After cleaving the fiber, it is important not to touch the cleaved part otherwise the cleaved surface is damaged reducing the splice quality.

Figure 4-4 (a) Fujikura FSM-50S fusion splicer (b) prepared fibers ready for splicing

In the second part of the splicing procedure, the prepared fibers are placed on the splicer. Figure 4-4(a) is the FSM-50S arc-fusion splicer that we used. In Figure 4-4(b) one can see the previously prepared fibers standing perpendicular to the electrodes that will create an arc during the splice operation. With this arc the two fiber ends, aligned by means of image processing, are melted/fused together.

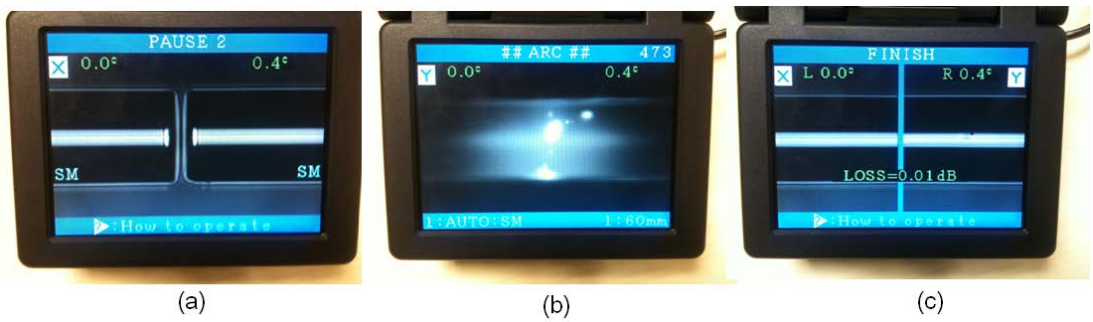

(a) (b) (c)

Figure 4-5 (a) alignment of fibers by image processing (b) fusion splice by arc created at tips of electrodes (c) loss estimation and proof test

After the fibers are placed in the splicer as in Figure 4-5 the fibers are aligned. Then, an arc is created across the electrodes, which melts the fibers and completes the splicing operation. Finally loss estimation by image processing is made and the spliced fibers are pulled away from each other around the splice point in order to make a proof test [53].

After the splice, it is preferable to make the splice point stronger. Recoating this part of the fiber with special UV-curable compounds is possible, whereas using splice sleeves, which shrink around the splice point when heated is also an efficient solution.

Using these methods, we assembled the FOG shown in Figure 4-6. The two Lyot depolarizers, discussed in previous chapters, are spliced at both entrances of the fiber coil.

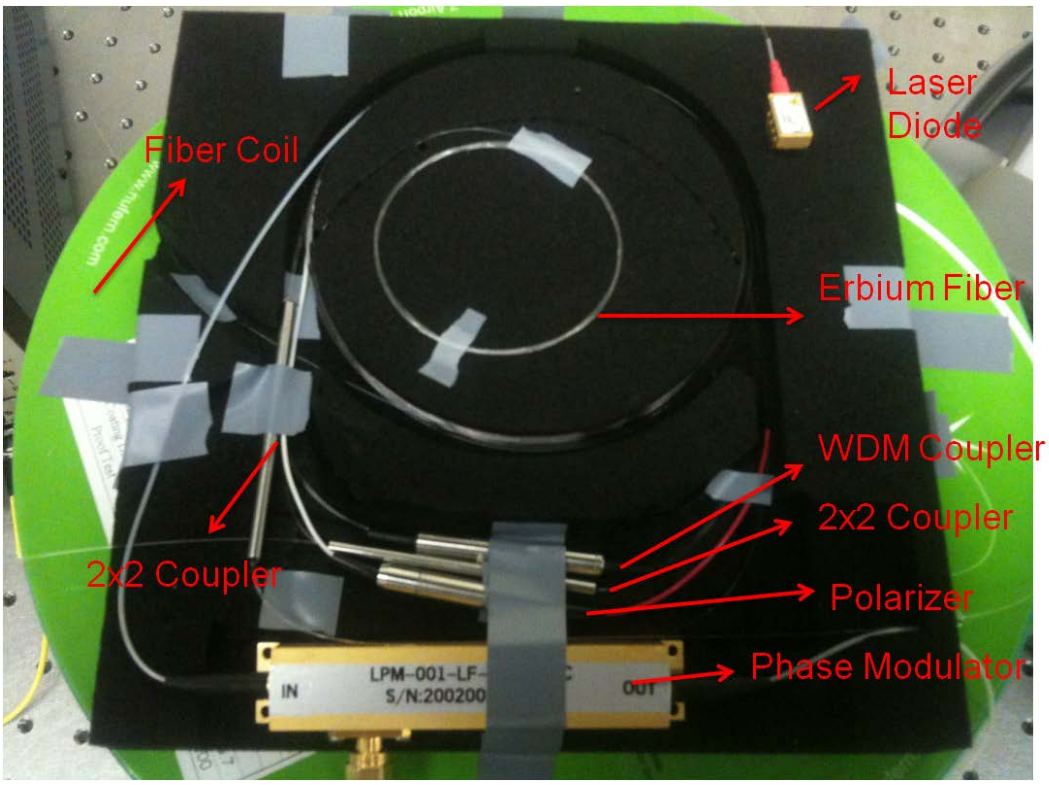

Figure 4-6 FOG components spliced together

4.1.2 Optical Spectrum Analyzer (OSA) Measurements of the Erbium Doped Superfluorescent Fiber Source

One needs to analyze the light source of the FOG configuration shown above. The first is the laser like 980nm light out of the laser diode and the second is the broadband 1550nm light emitted out of the Er-doped SFS. With the Yokogawa AQ6373 OSA located at TUBITAK SAGE laboratories (Figure 4-7) we checked whether the output of these two sources is as expected in theory or not.

Figure 4-7 Yokogawa AQ6373 optical spectrum analyzer

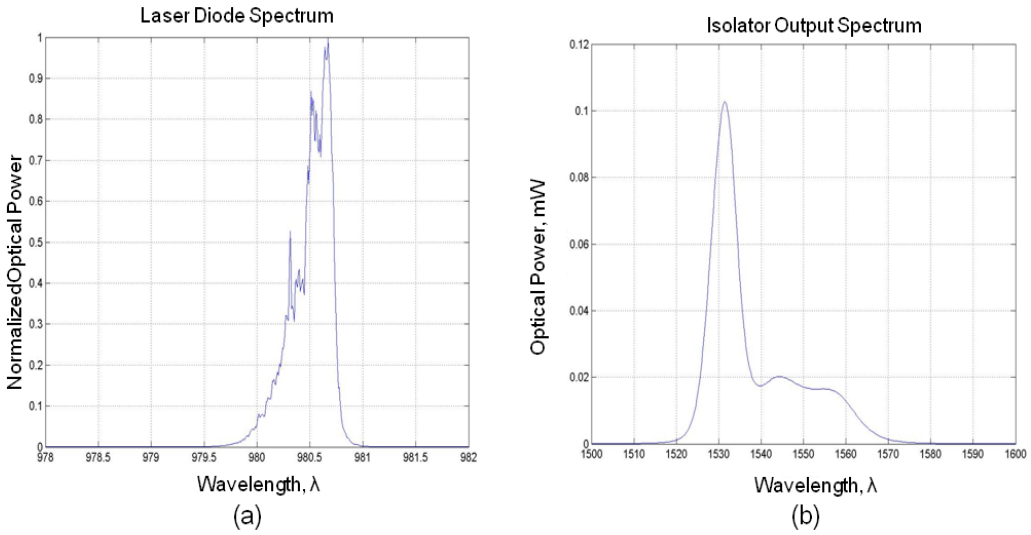

Figure 4-8 OSA measurements at the output of (a) 980nm laser diode (b) 1550nm Er-doped SFS

Spectrum width for the laser diode output is given as 2nm for the laser diode. This specification seems to support our measurement, as it is also the case for the broadband Er-doped SFS. In addition, we also checked the spectra for different pump currents (Figure 4-9).

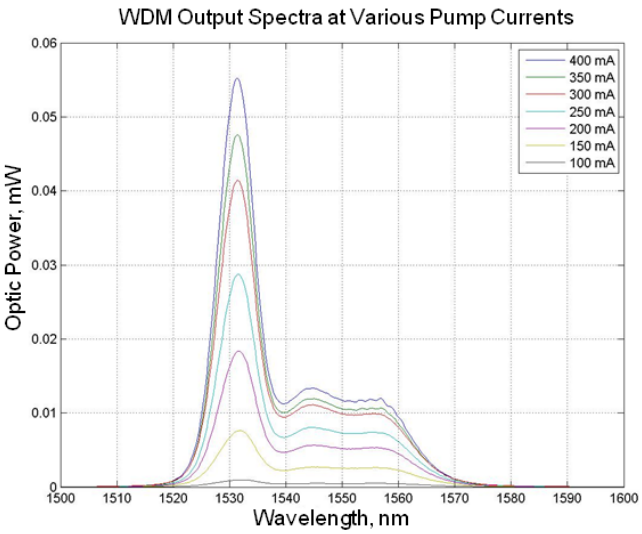

Figure 4-9 Optical spectra for various pump currents

After having verified the spectra of light propagating through our FOG system we can move on to the optical loss analysis.

4.1.3 Optical Loss Analysis

Optical power out of the light source had to be measured to undertsand loss in the system. During our tests, we used the Thorlabs ITC4001 Laser Diode/Temperature Controller to bias the laser diode (Figure 4-10)

Figure 4-10 Thorlabs ITC4001 laser diode / temperature controller

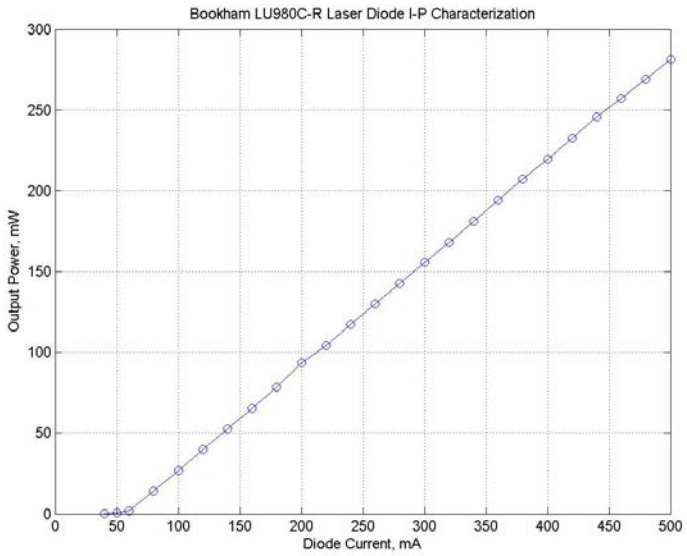

Figure 4-11 Laser diode I-P characterization

Laser diode that we used, as explained and verified before, emits a continuous light at 980nm. The pump current to optical power analysis is shown in Figure 4-11. Laser diode we used demonstrates quite a linear current to power characteristic.

Considering the smoother spectrum at the output of the WDM coupler (Figure 4-9) and the sufficient optical power around 155mW (Figure 4-11) we have chosen to work at 300mA pump current. Assembling our FOG we have made optical power measurements after each component. This measurement was done with a setup schematized in Figure 4-12.

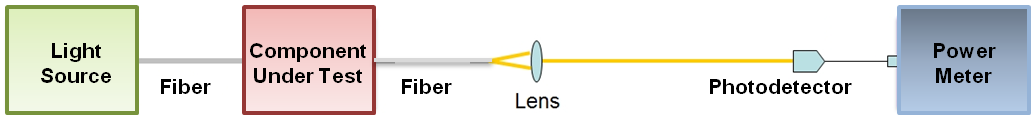

Figure 4-12 Optical power measurement setup

After each component is added to the system, the output of the last component is measured at 300mA of pump power. One critical point here is the following: Prior

to the measurement fiber ends have to be stripped, cleaned and cleaved in order to eliminate scattering from the end-face. Doing so we obtained the following;

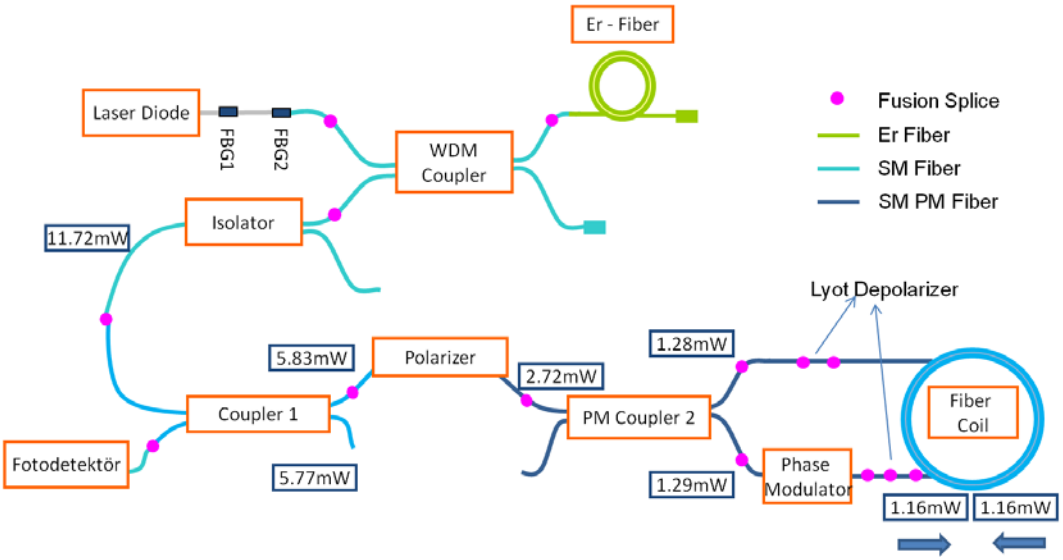

Figure 4-13 Optical power analysis of the FOG

Figure 4-13 is a visual representation of the optical power analysis of our FOG. Investigating this figure, we can conclude this section that optical power values after each component are reasonable which are consistent with theoretical foresights.

4.1.4 Polarization Extinction Ratio (PER) Analysis

Even though we use unpolarized light to circulate within the fiber coil, in order to apply the phase modulation, the light entering the phase modulator should be linearly polarized. Therefore, we need to check PER value at the output of the polarizer and PM coupler 2. Moreover, to reduce PNR errors created within the non-pm sensing coil we used Lyot depolarizers. This process should result in an unpolarized light at the output of the depolarizer. This was also proved with the PER measurement.

Despite the possibility of using an “out of the box” PER-meter, we preferred to perform PER measurements with our own setup (This set-up was built at the laboratories at TUBITAK).

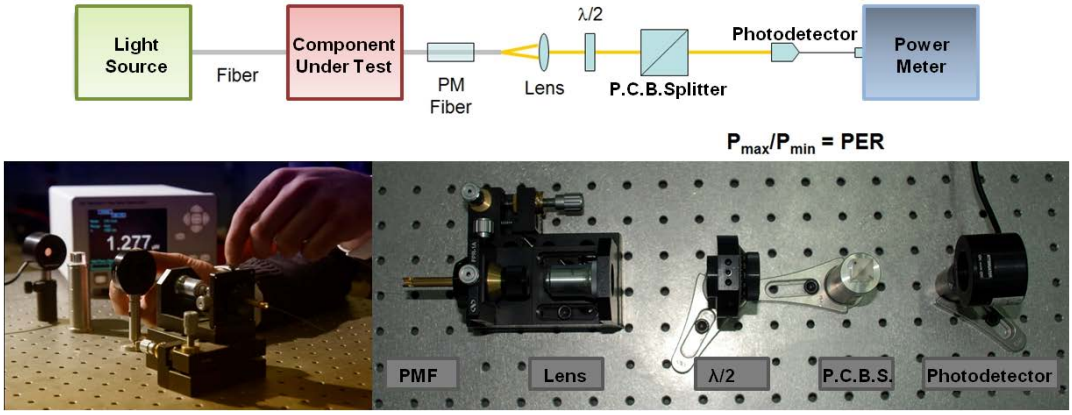

Figure 4-14 PER measurement setup

Figure 4-14 shows our PER measurement setup. PM fiber output of a polarizing or polarization maintaining component is inserted in a fiber chuck. Fiber chuck and the focusing (40x) lens are on an x-y alignment stage. With the use of an infrared (IR) detection card, light beam is directed and with the aid of the lens, focused on the detector. Then as the half-wave plate is rotated, polarization axes of the linearly polarized light are rotated as well. A polarization cube beam splitter (PCBS) is a bulk optical filter that filters out the TM mode polarization out of the side surface whereas the TE mode light incident on the PCBS is propagated through it. Therefore, as we rotate the half-wave-plate, we will read a maximum value when the sought after polarization component of light is incident on the detector. A minimum value is read from the power-meter when another 90º rotation of the half-wave-plate is performed. The measurement process explained above is clarified in Figure 4-15. Here the maximum optical power corresponds to the polarization that we want in our light that circulates in the FOG. Minimum value of the optical power defines the amount light coupled in the unwanted polarization axis. Therefore, the ratio between these two values gives the quality of the polarization of light. Speaking in a logarithmic scale, ten times the logarithm of this ratio gives the PER in dB units, equation(4.1).

$$PER(dB) = 10\log\frac{P_{\max}}{P_{\min}} \tag{4.1}$$

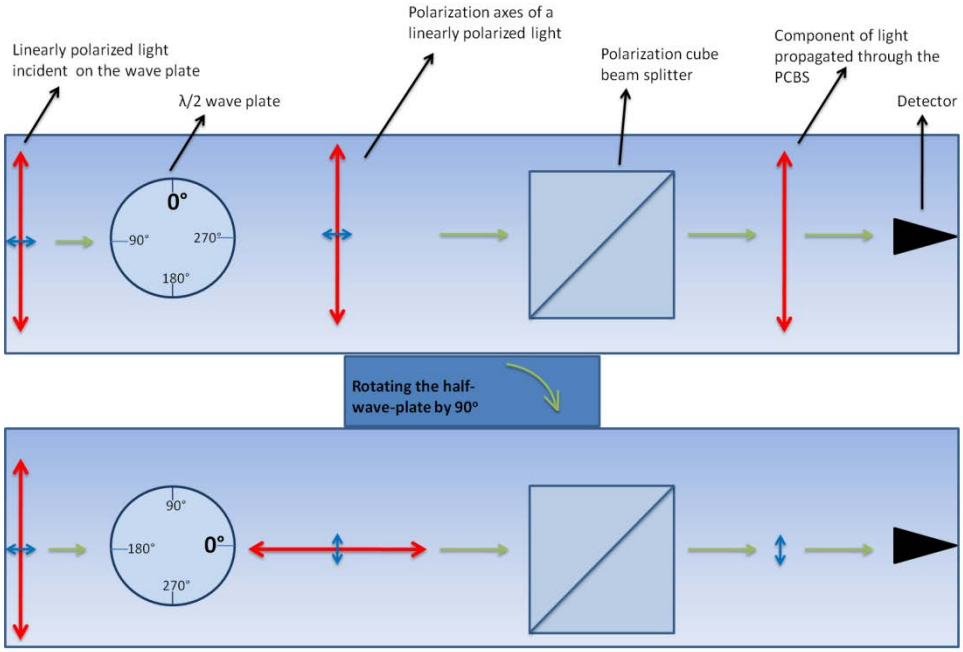

Figure 4-15 PER measurement procedure

Since we have explained the importance of polarization in FOGs and the concept of PER measurement up to this point, let us check our measurements. We performed our measurements with the Newport 1935-C power meter and a Newport 918D-IR detector.

Table 4-2 PER Measurements

Output	P_{max} (μW)	P_{min} (μW)	Ratio	PER (dB)
Polarizer	1996	1.4	1425.7	31.5
Coupler 2 (a)	940	1.1	854.5	29.3
Coupler 2 (b)	906	1.0	906.0	29.6
Phase Modulator	505	1.0	505	27.0

Analyzing the values obtained in Table 4-2 along with Figure 4-16 one can see that we have obtained reasonable values that were theoretically expected.

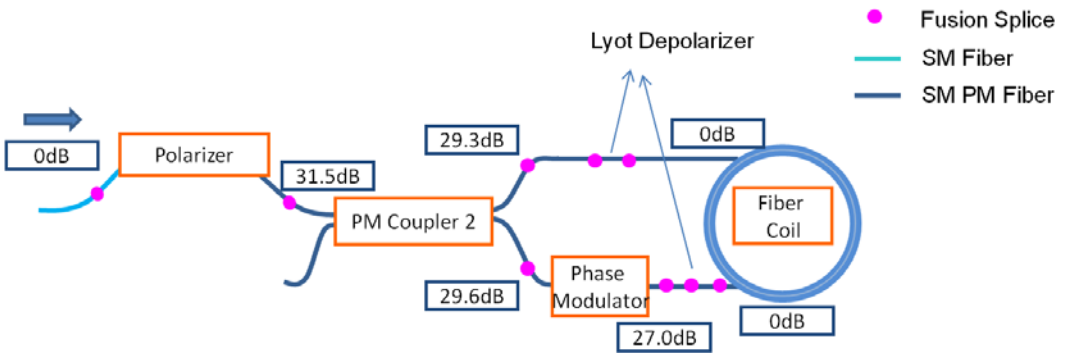

Figure 4-16 PER analysis of the FOG

Consequently, as expected the Lyot depolarizers have worked as expected totally randomizing the polarization of light passing through them without a noticeable power drop.

4.1.5 Optical Time Domain Reflectometry (OTDR) Measurements

In previous chapters, we examined the concept of the appropriate modulation frequency for the FOG. As explained, equation (2.14) gives the appropriate modulation frequency of the square wave applied to the phase modulator. In this equation, τ stands for the loop transit time of the light waves. In this case, we have to know the length of the loop in order to calculate τ. One method to this is to measure the length of the fiber with an OTDR. An OTDR is a device used to characterize an optical fiber. Using this device length and attenuation of the fiber can be measured. Briefly, an OTDR sends a pulsed light into the fiber with appropriate power and wavelength. Then it receives the backscattered and reflected light throughout and from the end of the fiber. According to the strength of these reflections and scatterings (Rayleigh backscattering) it determines the length and attenuation of the fiber under test.

In our measurements, we used the Yokogawa AQ7270 OTDR located at TUBITAK-SAGE laboratories (Figure 4-17).

Figure 4-17 Yokogawa AQ7270 OTDR

In order to calculate the appropriate modulation frequency we analyzed our fiber coil with this OTDR. As in the result in Figure 4-18, the coil length is measured as 4889.9m.

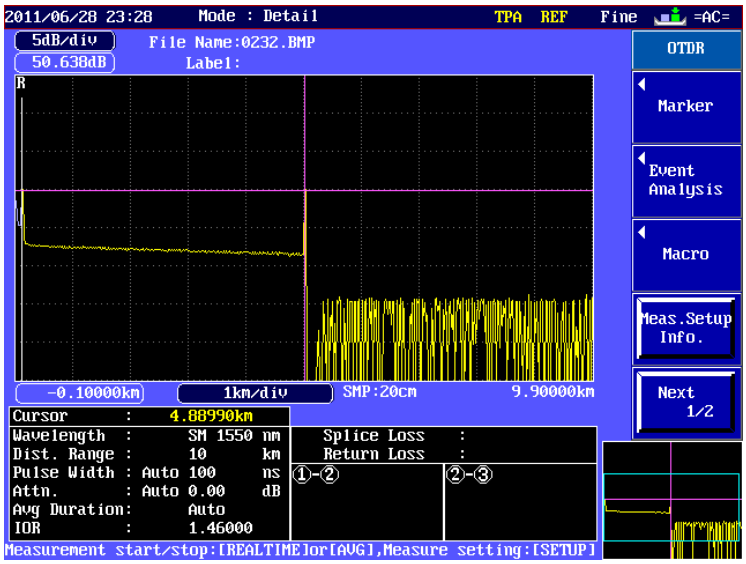

Figure 4-18 OTDR measurement of the fiber coil

The reason we chose to work with such a long length of fiber is to increase the sensitivity of our FOG. Parameters that determine sensitivity in a FOG are the

length of the fiber used and the diameter of the coil this fiber is wound around. In previous chapters we derived the Sagnac phase shift mathematically. In this equation (2.10) there is a limit to $\Delta\phi_s$. The FOG is modulated at ± π/2, from this points up to ± π only ± π/2 phase can be sensed in open loop FOG configuration, as in Figure 2-3, going beyond ± π on the interferogram detector power starts to increase again. Therefore, the limit to $\pm\Delta\phi_s$ is π/2. With this knowledge we can calculate the dynamic range of our FOG and compare it with other possible coil dimensions. Setting $\Delta\phi_s$ to π/2 in equation (2.10) we get Ω, which is the limit rotation rate that can be measured, as follows:

$$\Omega_{\max} = \frac{\lambda c}{4LD} \tag{4.2}$$

This result is in radians, to get the dynamic range in º/s this results has to be multiplied with $\frac{180}{\pi}$. With the FOG we assembled, the dynamic range according to equation (4.2) with L=4889.9m, D=0.15m, λ=1550nm and c=3x10^{8}m/s is 9º/s. However, if we used a fiber length of 200m and coil diameter of 2.5cm our dynamic range would be 1332 º/s.

Both dynamic ranges, ±9 º/s and ±1332 º/s are mapped to a region corresponding to ± π/2. Therefore we can conclude that as the multiple of LD increases the sensitivity of the FOG increases with a decreasing dynamic range.

4.2 The Measurement Setup

In this section, the system designed in the Optoelectronics laboratory at METU is explained. Furthermore, the transimpedance amplifier (TIA), which is the electronic circuit that converts the detector output (current) into voltage, is described as well.

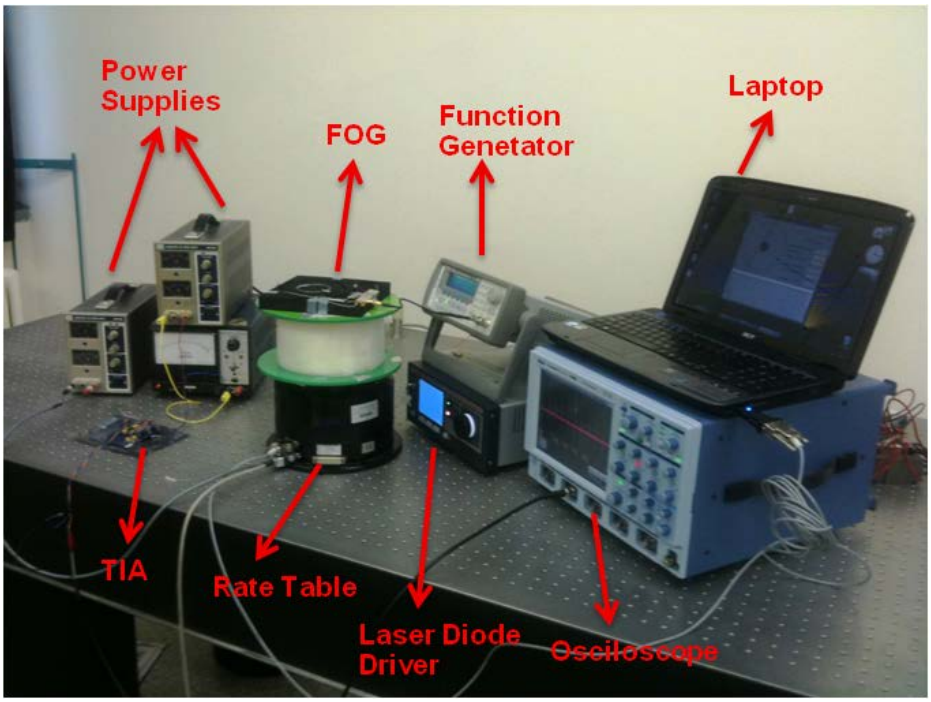

Figure 4-19 Test Setup

4.2.1 Peripheral Devices

After having assembled our FOG, we prepared the test setup (Figure 4-19) in order to collect data from the FOG to be post processed. We used power supplies to power the TIA and the rate table. A function generator was used to modulate light at the right frequency via the phase modulator. The laser diode controller was necessary to safely drive the laser diode. Furthermore, data was analyzed and collected with the digital oscilloscope and a laptop controlled the rate table.

Table 4-3 Peripheral Devices

Device	Make	Model
Power Supply 1	GW	GPR-3030 DC Power Supply
Power Supply 2	GW	GPR-3030 DC Power Supply
Power Supply 3	Kenwood	PR-602A DC Power Supply
Function Generator	Agilent	33220A
Laser Diode Controller	Thorlabs	ITC4001
Oscilloscope	LeCroy	6100A Waverunner
Rate Table	IMAR	iTES-PDT07

Devices that are used to operate the FOG are listed in Table 4-3.

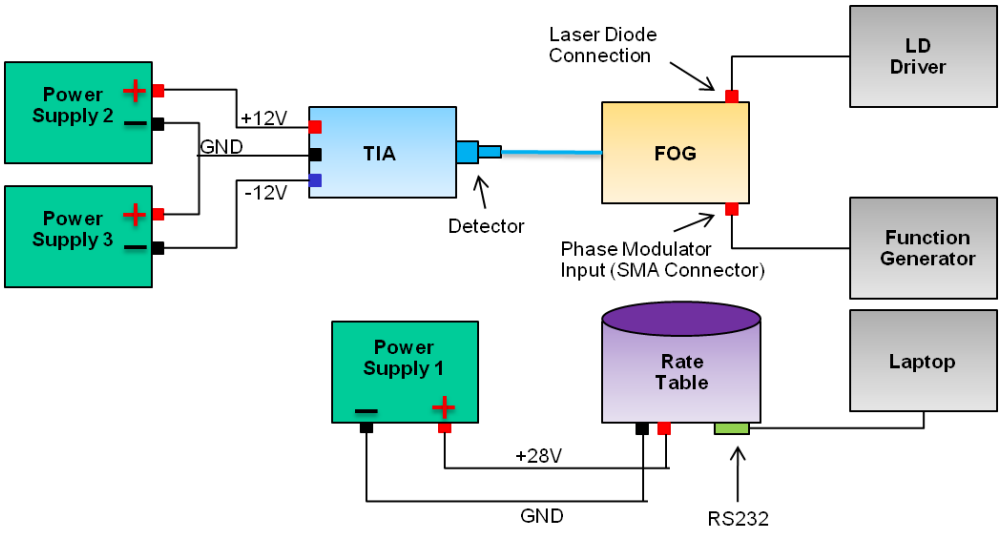

Figure 4-20 Test setup diagram

In order to generate the +12V, GND and -12V signals for the TIA we used two power supplies both set to output 12V. They are connected as it is in Figure 4-20. Since the detector of the FOG has to be soldered onto the TIA, it resides on the TIA circuit board. Another point that needs attention is the positioning of the sensing coil on the rate table. The sensing axis has to be perpendicular to the rate table surface. If not, measurements will not be correct.

4.2.2 Transimpedance Amplifier (TIA)

In electronics, a transimpedance amplifier is a current to voltage converter. The input impedance of a TIA is ideally zero. Therefore, current generated in the detector crosses a resistor that converts current into voltage. For this type of applications, FET-input operational amplifiers are used. We used the OPA657 by Texas Instruments, which is appropriate for photodiode applications using FOGs [54].

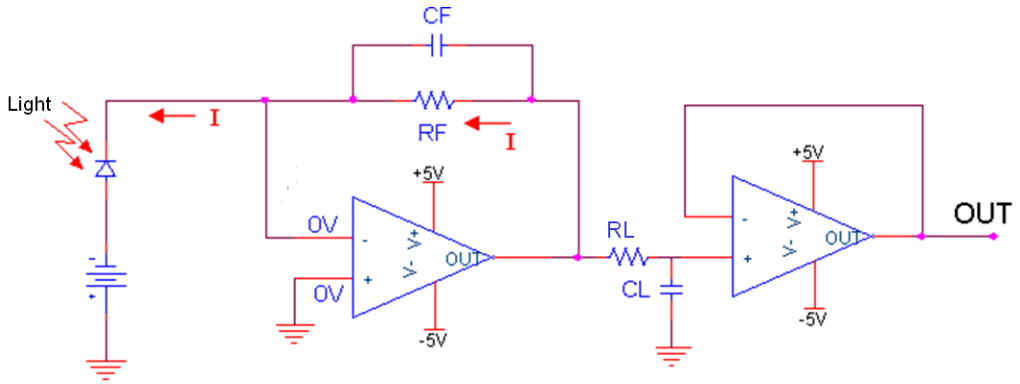

Figure 4-21 TIA Circuit

Figure 4-21 is the circuit we used to convert current from the photodetector to voltage. As it can be seen, the circuit designed at TUBITAK-SAGE consists of two stages. The first stage is the amplification and filtering stage (up to the second operational amplifier) and next comes the buffering stage, which aims to isolate the first stage from the analog to digital converter connected to the output. Both operational amplifiers in the figure are OPA657. As marked in the figure there is ideally no voltage at the input of the first operational amplifier. Therefore, all the current that sinks to the detector crosses the R_F resistor. The transconductance ratio (gain) of the TIA is expressed in ohms and corresponds to the value of the R_F resistor. Where C_F is the capacitance used to make sure that this configuration does not oscillate.

At the end of the first stage, there is an RC filter consisting of R_L and C_L. This low pass filter filters out noise coming from the optical components.

Table 4-4 Values for components of TIA

Component	Value
R_F	24.9 kΩ
C_F	1 pF
R_L	200 Ω
C_L	1 nF

According to Table 4-4 our gain is 24900 and the cut-off frequency of the filter, which is calculated by $f_c = \frac{1}{2\pi RC}$, is close to 800 kHz.

The second stage of the TIA circuit consists of a single OPA657. This prevents any degradation of the performance of the amplification and filtering stage when an analog to digital converter is connected to the output [54].

4.3 Testing the FOG

In this section, we describe the test on the assembled FOG. Prior to testing, we need to determine the correct V_π for the electro-optic phase modulator we use and the appropriate modulation frequency, which depends on the length of the fiber coil. Then we performed measurements by rotating the sensing coil on the rate table. Various input rates, positive and negative was applied to the fiber coil. Detector signals were read and saved from the oscilloscope to be post-processed on a PC later on. After having performed these tests with known rotation rates, we evaluated the scale factor of our FOG.

4.3.1 Calculation of the Appropriate Modulation Frequency

According to the length of the fiber that was measured with the OTDR, the appropriate modulation frequency can be calculated as discussed in section 2.2.3. The loop transit time, τ:

$$\tau = \frac{L}{c/n} \tag{4.3}$$

Where L stands for the measured length, c is the speed of light and n is the refractive index of the fiber. This value (taken from the Corning SMF-28e datasheet) is 1.46 for our fiber coil with SMF-e28 fiber. Therefore, substituting this into equation (2.14) we get:

$$f = \frac{c}{2nL} \tag{4.4}$$

Substituting correct values for c, n and L, the proper modulation frequency applied to our system is 21.010kHz.

4.3.2 Characterization of the Phase Modulator

There are two input parameters to the phase modulator. As explained, the phase modulator is driven using a function generator. One of the inputs is the previously calculated frequency of the square wave. In section 2.2, where we discussed rotation sensitivity and bias modulation we explained the necessity of modulating the light beams creating a phase differences of –π/2 rad and π/2 rad when there is no rotation. In order to do so, the amplitude of the modulation signal at the appropriate frequency should be $V_\pi/2$.

In case of no rotation of the platform and 0V input to the phase modulator, counter propagating waves will reach the detector in phase, resulting a constructive interference. In order to visualize this, one can check Figure 4-22. In case of such a constructive interference, detector power will be at its maximum. That is the red dot in Figure 4-22. As the input voltage increases, optical power at the detector will start to decrease. This is because of the interference of waves with some phase difference. At a certain point, detector power will reach its minimum possible value indicating there is a total destructive interference caused by a phase difference of V_π radians (green dot on Figure 4-22). Further increasing the modulation amplitude will cause the detector signal to return to the maximum value. This is an obvious result since light waves with 2π radians of phase difference will interfere constructively.

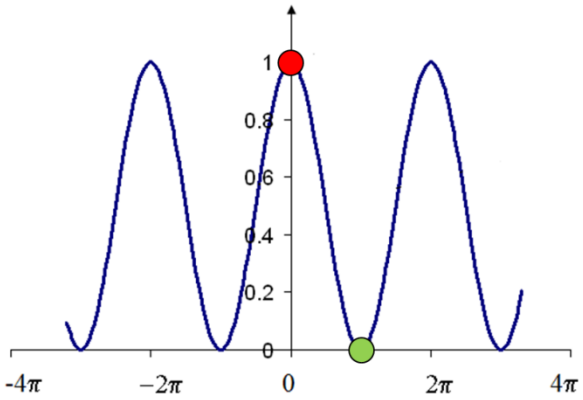

Figure 4-22 Interferogram at the detector

Therefore, half of the voltage applied to the phase modulator that causes the minimum input, can be taken as the $V_{\pi}/2$ parameter for our phase modulator.

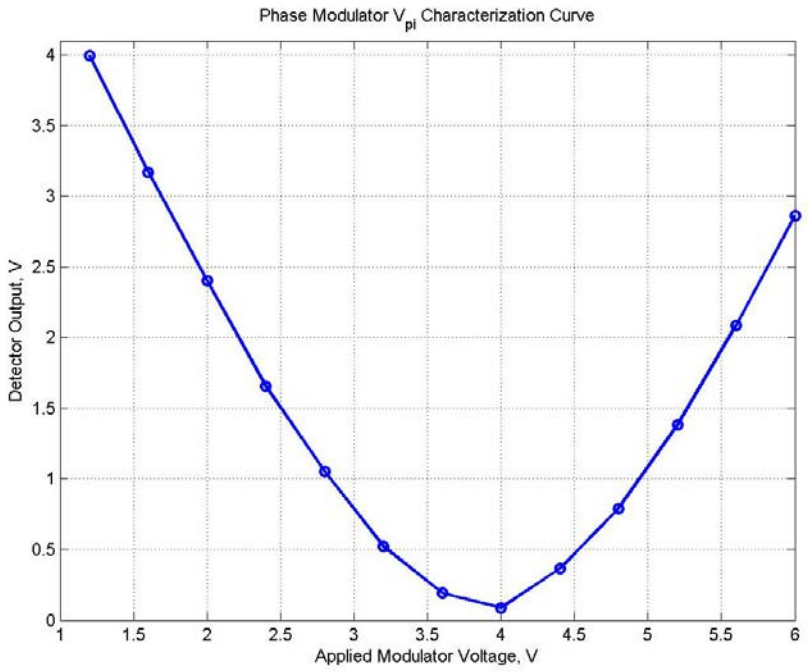

Figure 4-23 Phase modulator V_{π} characterization curve

We have applied the above-explained procedure to our FOG system, which was held stable causing no Sagnac phase shift between counter propagating waves. Starting from 0V, we increased the modulation amplitude with steps of 0.4V up to 6V.

The resultant applied voltage vs. detector output graph (Figure 4-23) is what we were expecting to see during the test. We can say that our phase modulator creates a phase difference of π radians at 4V, thus the required $V_\pi/2$ parameter required to operate our FOG is 2V.

After having determined the appropriate modulation frequency and the $V_\pi/2$ parameter for the phase modulator, we are ready to perform rate tests by rotating the FOG on the rate table.

4.3.3 Measurements with the Rate Table

Up to this point, we have dealt with the theory and assembly of the FOG. Now we will test the FOG by rotating it on the rate table (Figure 4-24). We applied input rates starting from -5º/s up to 5º/s by steps of 1º/s. Because of the square wave phase modulation nature, we expect to see detector outputs as in Figure 2-4.

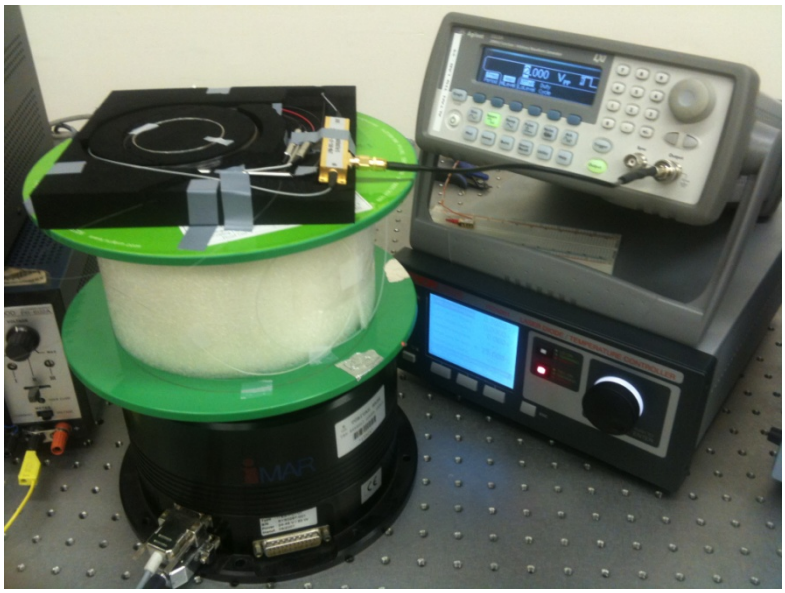

Figure 4-24 FOG on the rate table

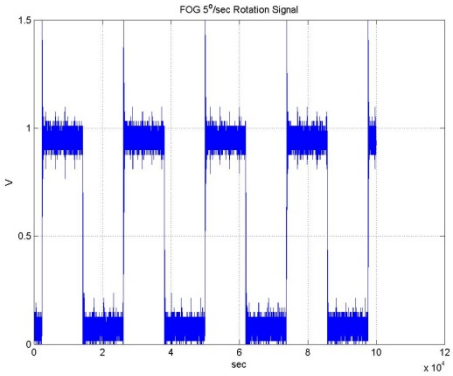

-5 º/s

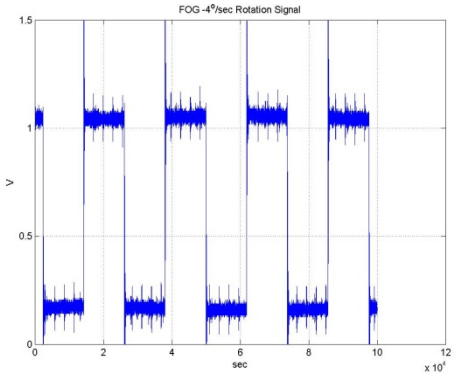

-4 º/s

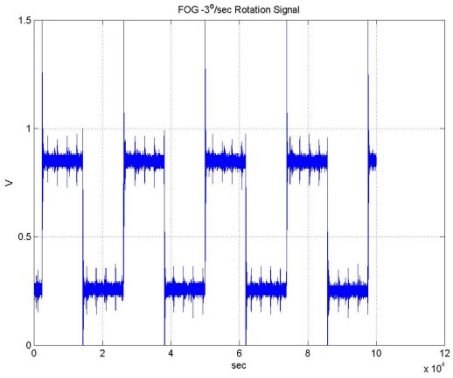

-3 º/s

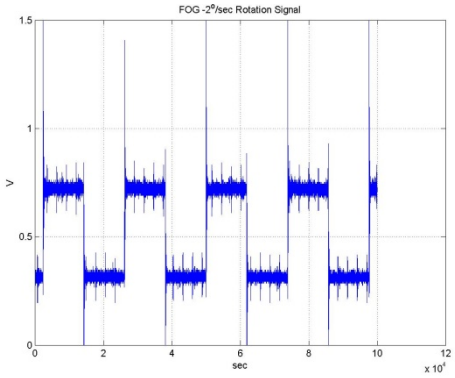

-2 º/s

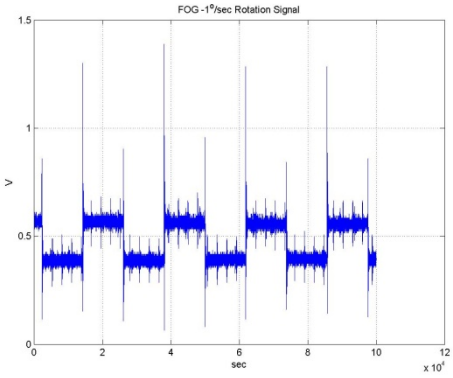

-1 º/s

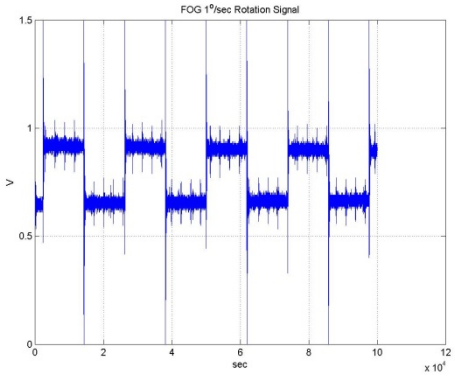

1 º/s

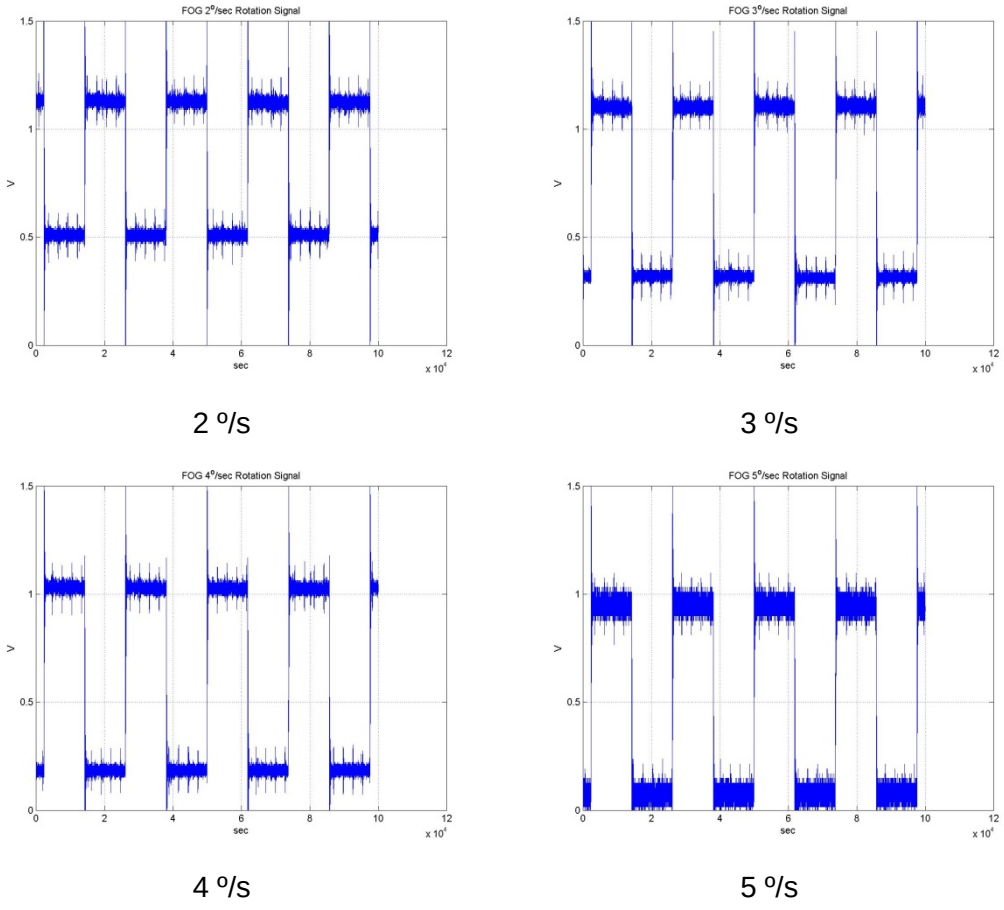

Figure 4-25 Output of detector at various rate inputs

Let us examine these graphs. Each graph obtained at a certain rotation rate is a square wave as expected. Upper levels of these graphs represent data collected when the operation point is at +π/2 and data at lower level of the square waves are collected when the operation point is at - π/2 (see section 2.2). This sequence becomes vice versa when direction of rotation of rotation changes. Therefore, training on direction of rotation is necessary before proper operation. As discussed before in the earlier chapters of this thesis, the difference of these two levels should be proportional to the input rotation rate. Since these data are points on the interferogram as shown in Figure 4-22, which is a sinus function, then the inverse sinus of the difference of these two levels will be proportional to

the rotation rate. For simplicity, let us call the values of the upper level of the square waves as D_u and ones on the lower level as D_l.

With the correct parameters input to the phase modulator and the reciprocal FOG configuration, we expect D_u+D_l to give the total power of the system. Since the total optical power of the system may change in time, we define the arcsine of the difference of these two levels normalized to the total power as proportional to the rotation rate:

$$Output = \arcsin\left(\frac{D_u - D_l}{D_u + D_l}\right) \tag{4.5}$$

By taking the ratio of the difference of the different levels to the total optical power counter propagating within the fiber coil, we eliminate the effect of change in optical power of the system. Converting the graphics in Figure 4-25 to values proportional to the input rate using equation (4.5) we obtain the following plot:

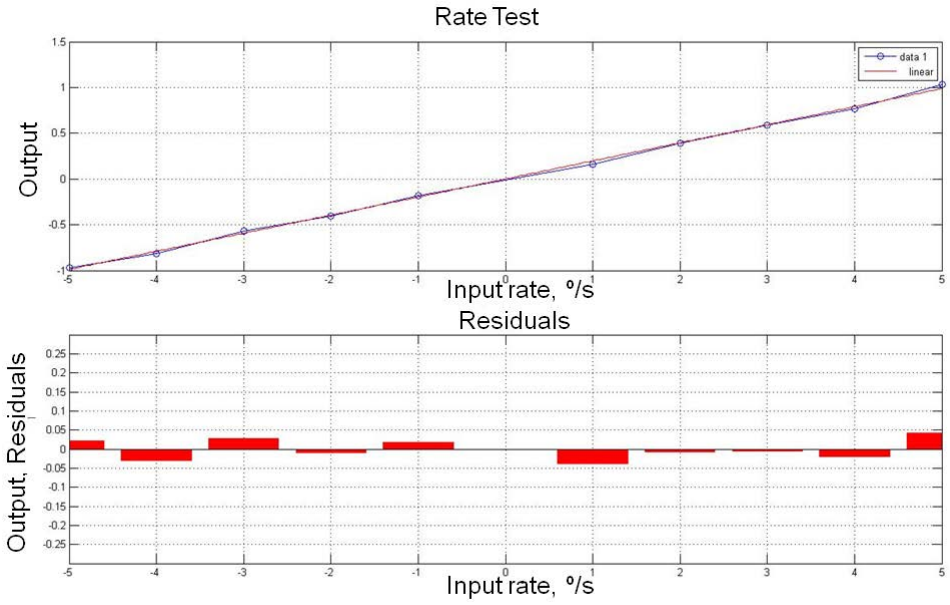

Figure 4-26 Input rate vs. output of the FOG

Figure 4-26 shows the input rates given to the FOG vs. the outcome of the system according to equation(4.5). In the lower figure, we can see the difference (residuals) of what we should have measured and what we have measured.

Table 4-5 Input rate vs. output of the FOG

Input	Output	Uncertainty
-5 º/s	-0.967	0.001
-4 º/s	-0.819	0.014
-3 º/s	-0.566	0.004
-2 º/s	-0.405	0.001
-1 º/s	-0.181	0.008
1 º/s	0.160	0.009
2 º/s	0.389	0.002
3 º/s	0.588	0.007
4 º/s	0.770	0.002
5 º/s	1.030	0.006

4.3.4 Experimental Evaluation of the Scale Factor

In this section, we will define the scale factor to the FOG we have designed and assembled. We will use the values in Table 4-5 to calculate the scale factor. As we have discussed before, the scale factor is a coefficient that relates the Sagnac phase shift to the rotation rate in degree/second unit.

Table 4-6 Scale factor for each rotation rate

Input	Output	Scale Factor
-5 º/s	-0.967	0.193
-4 º/s	-0.819	0.205
-3 º/s	-0.566	0.189
-2 º/s	-0.405	0.202

-1 º/s	-0.181	0.181
1 º/s	0.160	0.160
2 º/s	0.389	0.194
3 º/s	0.588	0,196
4 º/s	0.770	0,193
5 º/s	1.030	0,206

Examining Table 4-6, the mean scale factor for our FOG is 0.191 with a standard deviation of 0.014.

CHAPTER 5

DISCUSSION AND CONCLUSION

5.1 Conclusions

In this thesis, design and analysis of a fiber-optic gyroscope was presented. Fundamental concepts of the FOG such as reciprocity, bias modulation and the Sagnac effect are important concepts behind the working principles of the FOG. Afterwards, the components that are required to assemble a reciprocal FOG configuration are shown. Each component is explained, and details are given for alternative approaches along with their advantages and disadvantages. Finally, the steps taken and results obtained on a FOG system that was assembled is explained. Emphasis was given on the main part of the FOG, the phase modulator, and how recent advances in manufacturing have allowed these components to be miniaturized. Verification tests such as optical power analysis, PER measurements, OTDR measurements and OSA measurements are also given within the scope of this thesis.

The aim was to construct a FOG device using a 5km long spool of fiber, which can sense minute changes in rotation. It was observed that in order to construct this system care must be taken into fiber splicing, input power, spectral coherence of the light source as well as operation of the phase modulator. The majority of the system is designed in the Optoelectronics laboratory at METU while measurements and design of the necessary electronic components took place at the optical laboratories at TUBITAK-SAGE. The light source chosen to drive the system was an Er-doped SFS pumped by a 980nm laser diode. This broadband

light allowed us to eliminate interference effects due to coherence at the photodetector. Using the given fiber length (5km) the modulator was gated at a frequency of 21 kHz. Instead of using PMF in the fiber coil our system used SM fiber, and thus the input field into the coil was depolarized using Lyot depolarizers. This way interference effects were negligible. Using a polarizer, the field was polarized as it was sent into the electro-optic phase modulator. The necessary parameters to operate this device such as the proper modulation frequency (21kHz) and the $V_{\pi}/2$ value of the modulator (2V) are calculated and experimentally evaluated. After construction of the system, the entire set-up was placed on a rate table and the FOG measured rates as small as few degrees per second rates. The scale factor, which is a parameter that gives us an idea of the sensitivity of our system, was measured and calculated to be 0.191 with an uncertainty of 0.014. This large uncertainty (almost 7%) hinders us from measuring small rotation rates such as the rotation of the Earth, but allows us to understand the limits of such a system. The discrepancy is most likely due to our data acquisition system, where the noise in our measurements is too high to observe small rotation rates. It is possible to improve these results if the data is averaged over many cycles. Moreover, the cut-off frequency of the transimpedance amplifier that is used to convert current from the detector into volts can be arranged to have a lower value, closer to the proper modulation frequency. This would also decrease the noise in our measurements.

5.2 Future Work

In this thesis, a FOG was assembled and analyzed where the main focus was given on the fundamental concepts of the FOG. In other words, explanation of fundamental FOG concepts, discussion on components, alternative approaches and applied tests during assembly of the FOG was discussed in most of the thesis. One improvement that can be made is to add a fast data acquisition (DAQ) card to the system. Programming this DAQ card accordingly so that more averaging can be done will improve the uncertainty in the scale factor. In addition, collection of longer data (many hours) will allow us to apply more sophisticated data analysis methods. The Allan Variance method, which is one of these methods, requires long data acquisition from a stationary FOG. The

method can be used extensively to analyze the error characteristics and to measure and characterize the stability performance of any precision measurement instruments like clocks, oscillators, and systems for disseminating time and frequency. Various FOG parameters such as angle random walk that represents the noise of the output of the FOG and bias instability that represents the instability of the output of the FOG when there is no or some perfectly constant rotation can be obtained with this analysis [55]. Furthermore, it is possible to implement the IEEE Standard Specification Format Guide and Test Procedure for Single-Axis Interferometric Fiber Optic Gyros [56] when analyzing the FOG. This standard accepted by the IEEE association, describes various procedures for testing different parameters of the FOG. Finally, in this thesis our focus was on the straightforward open loop operation of the FOG. However, closed loop operation, which is more complicated and results in better performance, can be implemented to the FOG as well [49]. This technique, in general, uses the detector signal as a feedback to the phase modulator that aims to set the phase difference to zero using a serrodyne modulation technique [57] .

Although the system that was built in this thesis had very low rotation sensitivity, the operational principles and key attributes for successful operation of FOG devices was explained. The use of FOGs is very important for a wide array of applications. In Türkiye, FOGs are widely used in industry and military for different purposes. Various R&D projects on fiber-optics and MEMS gyroscopes have verified that sensitivities down to 1 °/h and more can be achieved. Typically, these sensitivity values are acquired with the use of PM fiber coils, fine-tuned electronics and closed loop FOG operation attributes which were discussed but not physically implemented here. Besides the assembly of a FOG with the above mentioned properties, production of the components used in FOGs play an important role in the development and production of the FOG device. It is desirable to manufacture all components of the device in-house in order to tailor devices to specific needs. Despite the fact that it is difficult to produce more sophisticated components such as the laser diode and specialty fibers (Erbium doped fiber, PMF), work is being done continuously to improve understanding and develop all manufacturing techniques necessary for autonomous development of these devices.

REFERENCES

1. Sagnac, G., "*L'ether lumineux demontre par l'effet du vent relatif d'ether dans un interferometre en rotation uniforme"* C. R. Acad. Sci., 1913, Vol. 95, pp. 708-710.

2. Michelson, A. A., and H. G. Gale., Journal of Astrophysics, 1925, Vol. 61, p. 401.

3. Rosenthal, A. H., "*Regenerative Circulatory Multiple Beam Interferometry for the Study of Light Propagation Effects.",* J.O.S.A., 1962, Vol. 52, pp. 1143-1148.

4. Macek, W. M. and Davis, D. T. M., "*Rotation Rate Sensing With Travelling-Wave Ring Lasers",* Applied Physics Letters, 1963, Vol. 2, pp. 67-68.

5. Ezekiel, S. and Knausenberger, G.E., "*Laser Inertial Rotation Sensors.",* SPIE Proceedings, 1978, Vol. 157.

6. Chow, W. W., et al., "*The Ring Laser Gyro",* Review of Modern Physics, 1985, Vol. 57, p. 61.

7. Vali, V. and Shorthill, R. W., "*Fiber Ring Interferometer",* Applied Optics, 1976, Vol. 15, pp. 1099-1100. (SPIE, MS8, pp. 135-136).

8. Lefevre, H. *The Fiber-Optic Gyroscope.* Boston : Artech House, 1993.

9. Stedman, G. E., "*Ring-Laser Tests of Fundamental Physics and Geophysics",* Reports on Progress in Physics, 1997, Vol. 60, pp. 615--688.

10. Pavlath, G. A., "*Fiber-Optic Gyroscopes",* IEEE, 1994. LEOS '94 Conference Proceedings. Vol. 2, pp. 237-238.

11. Schreiber, K. U., Klugel, T. and Stedman, G. E., "*Earth Tide and Tilt Detection by a Ring Laser Gyroscope",* J. Geophys. Res, 2003, Vol. 108, p. 2132.

12. Schreiber, K. U., et al., "*Direct Measurement of Diurnal Polar Motion by Ring Laser Gyroscopes",* Journal of Geophysical Research, 2004, Vol. 109.

13. Kung, A., et al., "*Rayleigh Fiber Optics Gyroscope",* IEEE Photonics Technology Letters, 1997, Vol. 9, p. 973.

14. Bergh, R, H.C, Lefevre and J., Shaw H., "*An Overview of Fiber-Optic Gyroscopes",* Journal of Lightwave Technology, 1984, Vol. 2, pp. 91-107.

15. Sagnac, G.C.R., "*L'ether lumineux demontre par l'effet du vent relatif d'ether dans un interferometre en rotation uniforme",* Compte-rendus de l'Academie des Sciences, 1913, pp. 708-710.

16. Liu, R.Y. and Adams, J.W., "*Interferometric Fiber-Optic Gyroscopes: A Summary of Progress",* Las Vegas, NV : IEEE, 1990.

17. Steven, J.S. Into the FOG: A Course on Fiber-Optic Gyroscopes. Ankara : Honeywell Technology Center, 2000.

18. Kaminow, I. P., "*Polarization in Optical Fibers",* IEEE J. Quantum Electron, 1982, Vols. QE-17.

19. Ulrich, R., "*Fiber-optic rotation sensing with low drift",* Opt. Lett., 1980, Vol. 5, pp. 173-175.

20. H.C., Lefevre, Bergh, R.A. and H.J., Shaw., "*All-fiber gyroscope with inertial navigation short-term sensitivity",* Opt. Lett., 1982, Vol. 7, pp. 454-456.

21. Lefevre, H., "*Fundamentals of The Interferometric FOG",* Photonetics, SPIE, Vol. 2837, pp. 2-15.

22. Pavlath, Dr. George A., "*Challenges in the Development of the IFOG",* Austin, Texas : AIAA Guidance, Navigation, and Control Conference and Exhibit, 2003.

23. K. Bohm, P. Russer and E. Ulrich, *"Low-noise fiber-optic rotation sensing"*, Opt. Lett., 1981, Vol. 6, pp. 64-66.

24. Böhm, K., et al., "*Low-Drift Fiber Gyro Using a Superluminescent Diode",* Electronics Letters, 1981, Vol. 17, pp. 352-353.

26. Wysocki, P.F., Digonnet, M.J.F. and Kim, B.Y., "*Spectral charactheristics of high-power 1.55um broad-band superluminescent fiber sources",* IEEE Photon. Technol. Lett, 1990, Vol. 2, pp. 178-180.

28. Wang, J.S., et al., "*High-power low-divergence superradiance diode",* Appl. Phys. Lett., 1982, Vol. 41.

29. Wysocki, Paul F., et al., "*Characteristics of erbium-doped superfluorescent fiber sources for interferometric sensor applications",* Journal of Lightwave Technology, 1994, Vol. 12, pp. 550-567.

30. Desurvire, E. and Simpson, J. R., "*Amplification of spontaneous emission in erbium-doped single mode fibers",* J. Lightwave Technol., 1989, Vol. 7, pp. 835-845.

31. Lefevre, Herve. *The Fiber-Optic Gyroscope.* 1993. p. 269.

32. Eickhoff, W., "*In-line fiber optic polarizer",* Electronics Letters, 1980, Vol. 16, pp. 762-764.

33. D. Gruchmann, K. Petermann, L. Staudigel, E. Weidel, "*Fiber optic polarizers with high extinction ratio",* 9th European Conference on Optical Communication (ECOC), 1983.

34. R. A. Bergh, H. C. Lefevre, H. J. Shaw., "*Single-mode fiber-optic polarizer",* Optics Letters, 1980, Vol. 5, pp. 479-481.

35. W. Johnstone, G. Stewart, B. Culshaw, T. Hart, "*Fiber optic polarizers and polarizing couplers",* Electronics Letters, 1988, Vol. 24, pp. 866-868.

36. Saleh, B. E. A. and Teich, M.C. *Fundamentals of Photonics (2nd edition).* New Jersey : John Wiley & Sons, Inc, 2007. p. 838. 978-0-471-35832-9.

37. Karna, Shashi and Yeates, Alan. *Nonlinear Optical Materials: Theory and Modeling.* Washington, DC : American Chemical Society. pp. 2–3. 0-8412-3401-9.

38. Hutcheson, L.D. *Intgrated Optical Circuits and Components.* s.l. : Marcel Decker, 1987.

39. Lefevre, H. C. et al, "*Integrated Optics: A Practical Solution for the Fiber-Optic Gyroscope",* SPIE Proceedings 719, 1986.

40. Yariv, Amnon and Yeh, Pochi. *Photonics, Optical Electronics in Modern Communication.* s.l. : Oxford University Press, 2007. p. 412.

41. Lefevre, Herve. *The Fiber-Optic Gyroscope.* Norwood, MA : Artech House, Inc., 1993. p. 276. 0-89006-537-3.

42. Wong, K. K., "*Integrated Optics and Optoelectronics",* SPIE Proceedings, 1990. Vol. 1374.

43. M. Izutzu, Y. Nakai, and T. Sueta, "*Operation mechanism for the single-mode optical-waveguide Y-junction",* Optics Letters, 1982, Vol. 7, pp. 136-138.

44. Hotate, Kazuo, "*Future Evolution of Fiber Optic Gyros",* 1A, 1997, Vol. 4, pp. 28-34.

45. S. Zafraniec, et al., "*Performance improvements in depolarized fiber gyros",* SPIE Proceedings, 1995, Vol. 2510, pp. 37-48.

46. K. Bohm, et al, "*Low-drift fibre gyro using a superlunimescent diode",* Electron. Lett., 1981, Vol. 17, p. 352.

47. Shupe, D. M., "*Thermally induced nonreciprocity in the fiber-optic interferometer",* Appl. Opt., 1980, Vol. 19, pp. 654-655.

48. Frigo, N. J., "*Compensation of Linear Sources of Non-Reciprocity in Sagnac Interferometers",* SPIE Proceedings, 1983, Vol. 412, pp. 268-271.

49. Culshaw, B, *"The optical fibre Sagnac interferometer:an overview of its principles and applications",* Meas. Sci. Technol., 2006, Vol. 17, pp. R1-R16.

50. Peterman, K., Bohm, K. and Weidel, E., "*Sensitivity of a fiber-optic gyroscope to environmental magnetic fields",* Opt. Lett., 1982, Vol. 7, pp. 180-182.

51. Hotate, K. and Tabe, K., "*Drift of an optical fiber gyroscope caused by the Faraday effect: influence of earth's magnetic field",* Appl. Opt., 1986, Vol. 25, pp. 1086-1092.

52. Ezekiel, S. and Davis, J. L., "*Techniques for shot-noise-limited inertial rotation measurement using a multiturn fiber Sagnac interferometer",* SPIE Proceedings, 1978, Vol. 157, pp. 131-136.

53. Yablon, A.D. *Optical Fusion Splicing.* 2005. 3-540-23104-8.

54. Texas Instruments, OPA657. *1.6GHz, Low-Noise, FET-Input OPERATIONAL AMPLIFIER.* 2001.

55. Yıldırım, Ali Galip., "*Guidance Control of a Missile With Noisy Inertial Sensors: Modelling of the Inertial Sensors and Analysis of Error Sources",* VDM Verlag Dr. Müller, 2010. ISBN-13: 978-3639243222.

56. IEEE. IEEE Standard Specification Format Guide and Test Procedure for Single-Axis Interferometric Fiber Optic Gyros. 1997.

57. *Serrodyne modulator in a fibre optic gyroscope.* J, Kay C. s.l. : IEEE Proceedings, 1985, Vol. 1132.